Universitat
de les Illes Balears

Title: Mesoscale oceanic convergence and divergence: Quasi-geostrophic theory, analytical modeling and observations

AUTHOR: Daniel Rodríguez Tarry

Master's Thesis

Master's degree in Advanced Physics and Applied Mathematics
(With a speciality/Itinerary Geophysical Fluids)

at the

UNIVERSITAT DE LES ILLES BALEARS

Academic year 2017-2018

Date: 4 July 2018

UIB Master's Thesis Supervisor: Ananda Pascual Ascaso

Abstract

Mesoscale oceanic features, like fronts, meanders, eddies, gyres, are characterized by temporal and spatial scales that range from a few days to several months and from a few meters to 100 km. Vertical motions associated with mesoscale motions play a key role in the ocean circulation and ocean-atmosphere interaction; supplying nutrients, conveying heat, salinity and momentum fluxes. However, the measurement of these vertical velocities represents a challenge, since they are three to four orders of magnitude smaller than the horizontal velocities. Traditional observing systems lack accuracy and resolution to capture the small scale signal of these vertical fields. Vertical motions are related to the horizontal convergence and divergence as a consequence of the continuity equation. In this master's thesis we study the convergence/divergence of a mesoscale eddy using two different approaches: an analytical model and Lagrangian observations.

We implement and evaluate a code based on an analytical model of baroclinic instability to generate fields of convergence/divergence. The code is written in Python and is made freely available through github. The model consists in a two-layer region where the upper layer has a constant shear flow and the bottom layer has no motion. It assumes quasi-geostrophic equilibrium and recreates the baroclinic instabilities that can be found in a region such as the Algerian Basin.

The Lagrangian observations used here were obtained by a set of drifters deployed at the south of Almeria (Western Mediterranean); which eventually got caught inside an eddy formed by a baroclinic instability of the Algerian Current. By studying the rate of change of the area of a parcel formed by a set of drifters, a calculation of the horizontal convergence/divergence is performed.

In order to compare both methods, we simulate an eddy with the properties of an eddy located at the Algerian Basin such as the sampled by the drifters. To obtain its hydrographical characteristics we use data from a glider, an autonomous underwater vehicle that sampled the same eddy. In addition, to corroborate the origin of the eddy as an instability of the Algerian Current, we use satellite altimetry data to track its origin.

Both results are analyzed and a discussion between the different methods and its value to the calculation of convergence/divergence zones is provided. Ultimately, we estimate vertical velocities from the model and compare with those obtained from the glider data set using the omega equation within the Quasi-geostrophic approximation.

Index

1 Introduction

1.1 Motivation

Vertical movements of water associated with mesoscale motions, from the surface to the depth across the base of the mixed layer, play a key role for the transport of properties (like heat and salinity), gases, biogeochemical tracers, momentum fluxes and fate of drifting particles/ objects as debris and pollutants. Typical scales of mesoscale features ranging from a few days to several months and from a few meters to 100 km represent a challenge to their observation and study. Until recently, meso and submesoscale structures had not received much attention due to the difficulty generated by its observation and modeling (Mahadevan & Tandon, 2006). The measurement of the vertical velocities represent a challenge, since they are three to four orders of magnitude smaller than the horizontal velocities. Traditional observing systems lack of enough accuracy and resolution to capture the small scale signal of these vertical velocity fields. Only vertical velocities greater than 1000 m day^{-1} are observable directly with Eulerian measurements. Assuming Quasi-geostrophic balance (hereafter QG), among other limitations, allow to estimate vertical velocities of smaller orders down to O(10 m day^{-1}) (Tintoré et al. (1991) and Pascual et al. (2004) for details). This involves computational derivatives of observed fields which incorporate errors to the results, due to the distribution of these observations and also the inherited lack of synopticity. The balance between the number of observations and the synopticity of observations affects the apparent flow and in particular the diagnosed vertical motion. A combination of effects can typically lead to errors over 50 % in the estimation of net vertical heat flux (Allen et al., 2001; Gomis et al., 2005).

Taking account of the difficulties exposed, there are critical questions that have not been answered yet, like which are the properties from the surface boundary layer exported to depth, which coherent pathways enable this exchange or how are these 3D Lagrangian trajectories. In this context, AlborEx and CALYPSO are two multi-disciplinary research experiments aimed at studying the of meso and submesoscale interactions. Both experiments are located in the Southwest Mediterranean Sea (Alboran Sea), a region characterized by sharp gradients that lead to the formation of intense gyres with associated intense vertical motions.

Vertical motions associated to mesoscale can be diagnosed from zones of convergence and divergence through the continuity equation. This equation in the form of eq. 1 shows the divergence term on the left hand side while on the right hand side expresses the vertical variation of the vertical velocity. In this equation x is the distance easward, y the distance northward, z the depth, u the zonal component of the velocity, v the meridional component and w the vertical velocity. The obtaining of a good description of the divergence field is crucial in order to estimate the vertical motions associated to it. The objective of this master's thesis is to analyze two methods of convergence/divergence calculation, in other words, two different approaches to the same problem.

$$\frac{du}{dx} + \frac{dv}{dy} = -\frac{dw}{dz}. \tag{1}$$

Firstly, we implement and evaluate a code based on one of the two baroclinic instability models proposed by Tang (1975). This code, written in Python (TangPy, hereafter), resolves analytically the dynamics of a two-layer fluid with a stratified shear layer over a quiescent stratified layer. This simplified QG model presents some advantages such its manageability and low computational cost. The ability of TangPy to produce instantaneous results allows the assessment of the spatio-temporal

evolution of the fields with different parameters almost with no time cost, a clear advantage in front of other numerical models like WMOP or CMEMS which take much more time to run. Despite of its simplicity, Tang's model has still been used until now with solid results (Gomis et al. (2005); Flexas et al. (2001); Sammari et al. (1994);). If an appropriated region is selected, as QG is a valid approximation in the open water (Buongiorno et al. (2012); Pascual et al. (2015)). The model presented in Tang (1975) only gives an analytical solution for the stream function and vertical velocity field, however in this work we have extended the outcome by adding the solutions for the velocity, divergence and vorticity fields.

Secondly, we study a method proposed firstly by Reed (1971) and later expanded by Molinari and Kirwan (1975) based on the rate of change of the area of a parcel formed by a cluster of drifters. By this method, values of convergence/divergence can be calculated by using only Lagrangian observations. Unfortunately, the literature about the use of this method is not vast and only a few authors have used it (Molinari and Kirwan (1975); Okubo and Ebbesmeyer (1975); Wang et al. (1988); Niiler et al. (1989); LaCasce and Ohlman (2003)). Therefore, there are still open questions. However, recently, part of the oceanographic community has made an effort to answer some of these open questions (Poje et al. (2014); D'Asaro et al., (2017); project CALYPSO). In this work we apply this method to a cluster of drifters deployed in the frame of the AlborEx experiment.

The novelty of this master's thesis is the combination of the two aforementioned approaches in the study of a mesoscale eddy. The combination of Eulerian and Lagrangian resolution for the same phenomena is not a common procedure (in general, studies only apply one of the two procedures). The phenomena studied in this work will be a mesoscale eddy located in the Algerian Basin (hereafter AB) developed from an instability of the Algerian Current (hereafter AC, see Fig. 1). These structures, also known as Algerian Eddies (hereafter AEs), are almost always present in the basin and play a key role in its circulation (Testor et al. (2005); Escudier et al. (2016)). AEs are generated from the AC due to a mixture of both barotropic and baroclinic instabilities even though the second ones play a main role. As a result, we can apply TangPy to simulate the main dynamical fields. To estimate the input parameters of the model we will make use of glider data from a mission that sampled this AE (Cotroneo et al. (2015)) and satellite altimetry. For the Lagrangian observations we will use, as mentioned before, a cluster of drifters deployed in the AlboreEx experiment. Although these drifters were deployed in the Southwest of the Mediterranean sea, they got inside the AC and eventually drifted until the location of the AE and got inside its circulation. As there is a time gap between the drifter observations (end of May, beginning of June) and glider measurements (October) we made use of the altimetry data to confirm that we are studying the same feature.

This master's thesis is organized as it follows: First, a brief description of the area of study and a brief description of the origin of these regions of convergence/divergence is given. Section 2 describes the data used in this work followed by Section 3 where the methods used are exposed. In Section 4 the results are shown for the Lagrangian observations and for the Tang' model. A brief discussion of some interesting points of the results in Section 5. Section 6 and Section 7 summarize the work done and suggest future work in order to improve the understanding of the results shown.

1.2 A case of study: an Algerian Basin Eddy

As said before, we apply the two methods in an eddy observed in the AB developed from an instability in the AC. To fully understand the mechanisms that set up this phenomena it is important to understand first the mesoscale circulation of the basin.

The Algerian Basin covers most of the southern part of the Western Mediterranean Sea so in order to understand its general circulation we have to look up to the full region. The Mediterranean Sea is a semi enclosed basin as it is a confined region only communicated with the Atlantic Ocean through the Gibraltar Strait. The unbalance caused by a greater evaporation than precipitation and river runoff is compensated by the strong inflows of Atlantic waters into the basin. The strong baroclinic and barotropic instabilities present at the zone studied in this work (Alboran Sea) cause the inflowing waters to form a sequence of eddies, gyres of high intensities (Allen et al., 2008). As these waters get out of the Alboran Sea they flow eastward at surface along the Algerian slope creating the AC. This is the beginning of the Mediterranean circulation in the uppermost part of the water column , an anti-clockwise circulation due to the Coriolis effect (Fig.1).

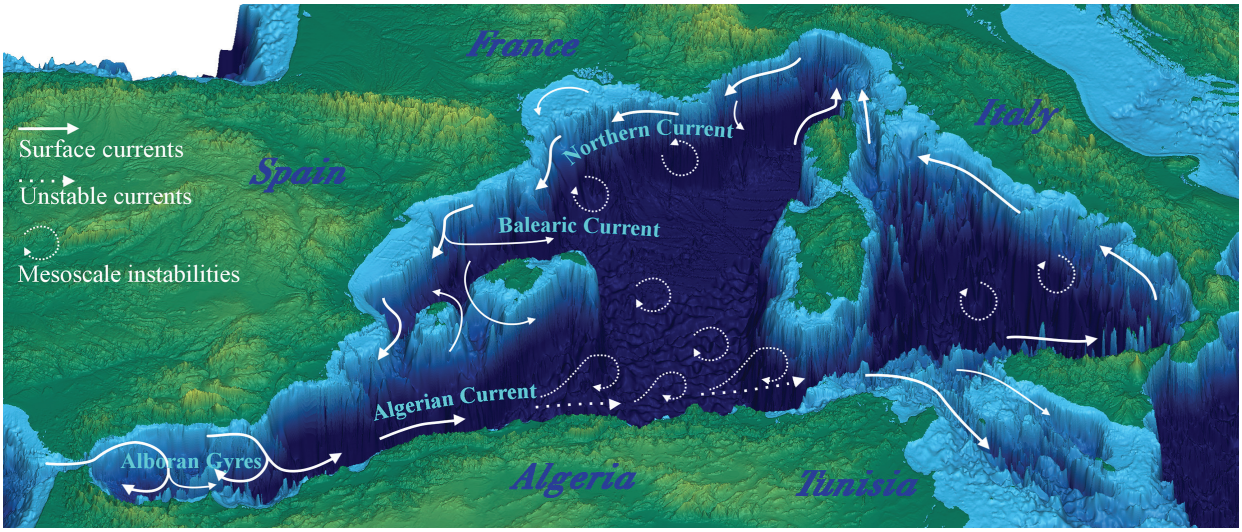

Figure 1: Schematic representation of the Western Mediterranean circulation (Escudier et al. (2016) adapted from Millot and Taupier-Letage (2005)).

When following the Algerian slope, the AC becomes unstable causing the formation of meanders which eventually can detach from the AC forming AEs (Salas et al. 2001). These eddies can rapidly grow to up to 50-100 km in diameter and reach vertical extent of several hundreds of meters (Ruiz et al., 2002). These structures retain much of their core water mass and consequently can last for numerous weeks, months or even years with few changes to their hydrographical characteristics (Millot et al., 1999).

1.3 Current instabilities

There is an inherent ability in the midlatitude eastward flows to generate spontaneously wave-like disturbances that can evolve an eastward stream into a meandering state (Kundu,2008). The meanders formed on the current frequently can grow, closing onto themselves and form eddies that separate from the main current. As mentioned before, such a change on the current is the result of a mixture of barotropic and baroclinic instabilities. Barotropic instabilities withdraw the kinetic energy from the horizontally sheared flow to feed the meander grow. On the other hand, the baroclinic instability is associated with a conversion of available potential energy from the horizontal density distribution in balance with the thermal wind. Occasionally, beta effect (first order term of the Coriolis approximation and sets a linear variability with latitude) plays a role too helping the eddy to detach from the current (Cushman-Roisin, 2011). In this work we will focus on the

baroclinic instability as a generation method of AEs.

In thermal-wind balance, geostrophy and hydrostaticity combine to maintain a flow in equilibrium, although this state is not the state with least energy as we have a system with inclined density surfaces. According to the thermal-wind relation (eq. 2),

$$\frac{\partial v}{\partial z} = -\frac{g}{\rho_0 f}\frac{\partial \rho}{\partial x}, \tag{2a}$$

$$\frac{\partial u}{\partial z} = \frac{g}{\rho_0 f}\frac{\partial \rho}{\partial y}, \tag{2b}$$

where u and v are the velocity components, x the distance eastward, y the distance northward, z the depth, ρ the density, g the gravitational acceleration at surface and f the Coriolis parameter at a reference latitude. An eastward flow in equilibrium with such a density structure must have a velocity that increases with height. This system is potentially unstable as it can release the potential energy stored in the slopes of the density surfaces, reducing the pressure gradient and therefore the vertical shear of the main flow; thus, transferring this energy into the kinetic energy of the perturbations.

In thermal-wind balance this energy transfer cannot happen spontaneously so some mechanism is required: (i) through friction, a state of thermal-wind balance can decay and eventually bring the system to rest. However this mechanism is too slow. (ii) Vertical stretching and squeezing of the fluid can help to change positions of parcels of different densities, reducing the slopes of the density surfaces. Vertical stretching and squeezing, each by itself, generate a vorticity wave, but only if the mechanisms induce a pattern that reinforces each other (Fig. 2). If this happens, a partial relaxation of the density surfaces liberates some of the potential energy available while the two mechanisms create new vorticity. The motions produced by the generation of kinetic energy increase the amount of vorticity shear enhancing the action of the friction which also contributes to the reduction of the slopes of the density surfaces. With time, large vortices which eventually can detach and form an eddy can be generated at expenses of the initial thermal-wind balance.

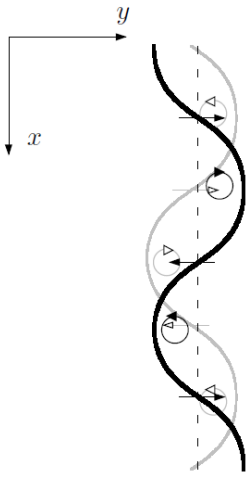

Figure 2: Interaction of displacement patterns and vortex tubes in the upper layer of a two-layer thermal-wind flow when displacements occur in both layers. The illustration depicts the case of a mutually reinforcing pair of patterns, when the vertical motions of one pattern act to increase the displacements of the other (Cushman-Roisin, 20011).

2 Data

2.1 Drifters

The Lagrangian observations used in this study were obtained during the AlborEx campaign, conducted in the eastern Alboran Sea front in May 2014 (Pascual et al., 2017). The Surface Velocity Program (hereafter SVP) drifters are the standard design of the Global Drifter Program (Lumpkins and Pazos, 2007). In particular, the drifters used here are the mini-World Ocean Circulation Experiment (WOCE) SVP drifters (Fig. 3). The drifter consist of a surface buoy that is attached to a holey-sock drogue, centered at a depth of 15 m, which holds the drifter almost motionless with respect to the horizontal layer studied. The drifters were equipped with a thermistor on the lower part of the buoy to measure SST. The drifters were localized by GPS and transmitted data through Iridium connection. For more details on the SVP drifters design, see Niiler et al. (1991).

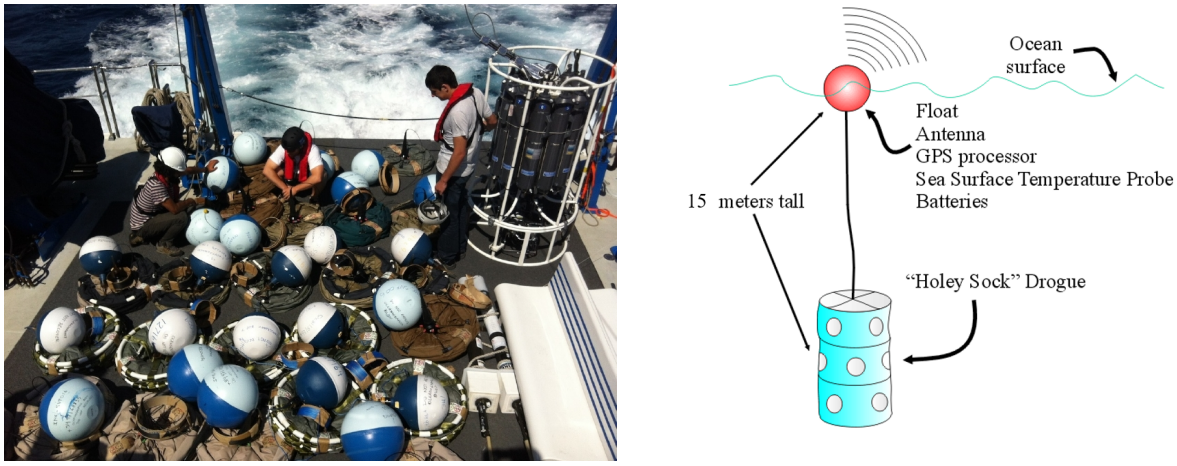

(a) (b)

Figure 3: (a) Drifter preparation on board R/V SOCIB during AlborEx experiment. (b) SVP drifter scheme.

In the AlborEx experiment, 25 drifter were deployed in the eastern Alboran Sea, far away from our region of study (Fig. 4b), but as they were deployed in the eastern part of the Almeria-Oran front, they got advected into the AC. This strong current transported the drifters into our region of study (AB). At this location, the presence of a strong instability from the AC deviated the drifters into an anticyclonic eddy, the case studied in the present work.

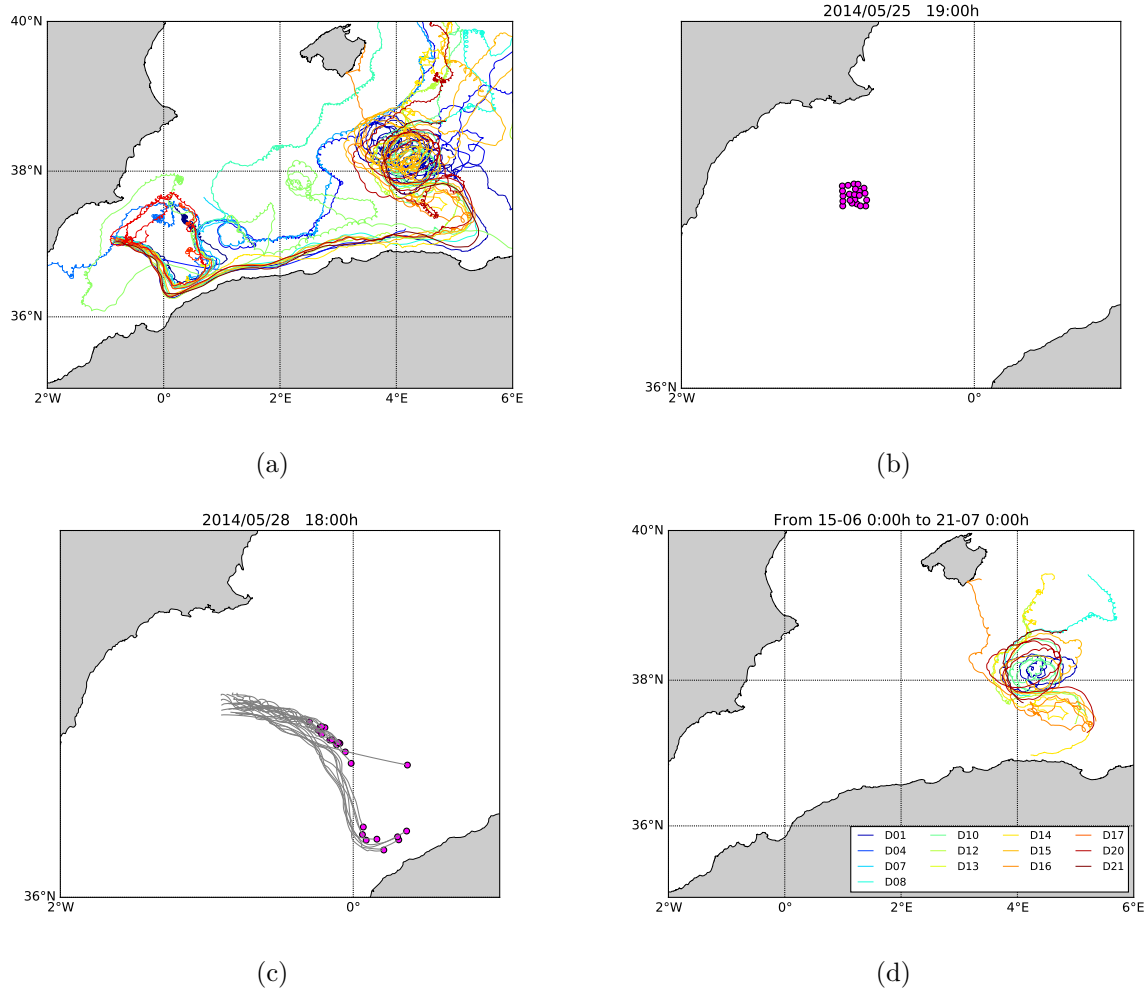

Figure 4: (a) Complete drifter trajectories (each color represent a drifter). (b) Drifters position when the deployment was finished. (c) Drifters derivation after 3 days. (d) Trajectories from drifters that sampled the eddy.

2.2 Glider data

Gliders are autonomous underwater vehicles that provide high-resolution hydrographic measurements (temperature, salinity, biogeochemichal tracers, etc). Gliders control their buoyancy to allow vertical motion. Making use of their ability to modify its pitch, together with their fins, gliders transform part of this vertical motion into horizontal motion, advancing with a horizontal speed around 25 cm/s (Bouffard et al., 2010). Following a saw-tooth flight path glider sample ocean down to 1000 m (Fig. 5b).

The glider data used here corresponds to the mission ABACUS2 in the ABACUS framework, a project carried by the University of Naples "Parthenope" in collaboration with the Balearic Islands Coastal Observing and Forecasting System (SOCIB) together with the Instituto Mediterráneo de Estudios Avanzados (IMEDEA CSIC-UIB) (Cotroneo et al., 2015). In October 2014, a glider SLOCUM G2 sampled two cross-sections of an eddy present in the Algerian Basin that got detached from the AC (Fig. 5c). ABACUS2 dataset is used to identify the the hydrographic characteristics of the studied eddy. This information is used to estimate the input variables for the TangPy code

(see section 3.1.1).

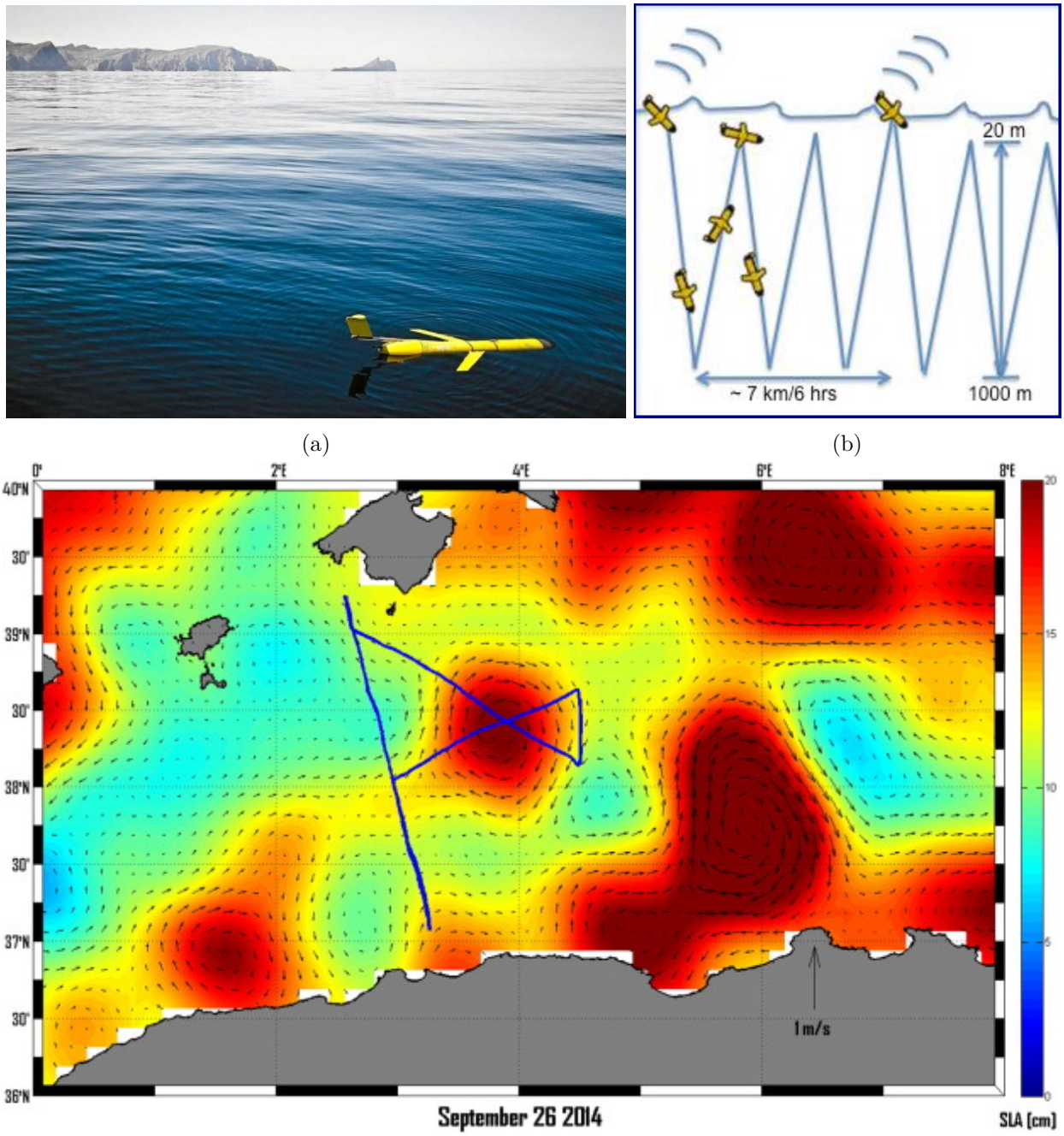

(a) (b)

(c)

Figure 5: (a) Glider waiting for communications before submergence. (b) Typical glider flight path under water. (c) Glider trajectory through the eddy from 15 September to 20 October 2014 (Cotroneo et al., 2015).

2.3 Satellite data

Altimetry data over the region of the Algerian Basin is used to confirm the origin of the mesoscale AE. Satellite altimetry measures the time taken by a radar pulse to travel from the satellite to the surface and back to the satellite receiver (Fig. 6). Combined with precise satellite location data, altimetry measurements yield sea-surface heights. The altimeter products used for this study were produced by Ssalto/Duacs and distributed by Aviso, with support from CNES (http://www.aviso.altimetry.fr/duacs/). More specifically, daily maps of Absolute Dynamic Topography (hereafter ADT) and geostrophic currents from late May 2014 to October 2014 are used.

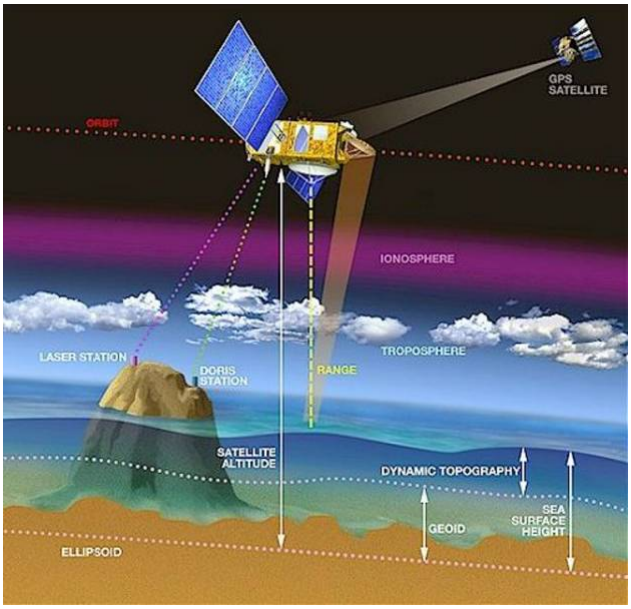

Figure 6: Scheme of the altimetry detection (https://www.aviso.altimetry.fr/en/).

Fig. 7 shows the distinct phases of the eddy, since its birth until its stabilization at the Southeast of Mallorca where it is sampled by the glider in early autumn 2014. In late May there is a strong baroclinic instability and as a result, a the AC deviates into a big meander. During the beginning of June a small perturbation of this meander is detached, forming a mesoscale eddy.

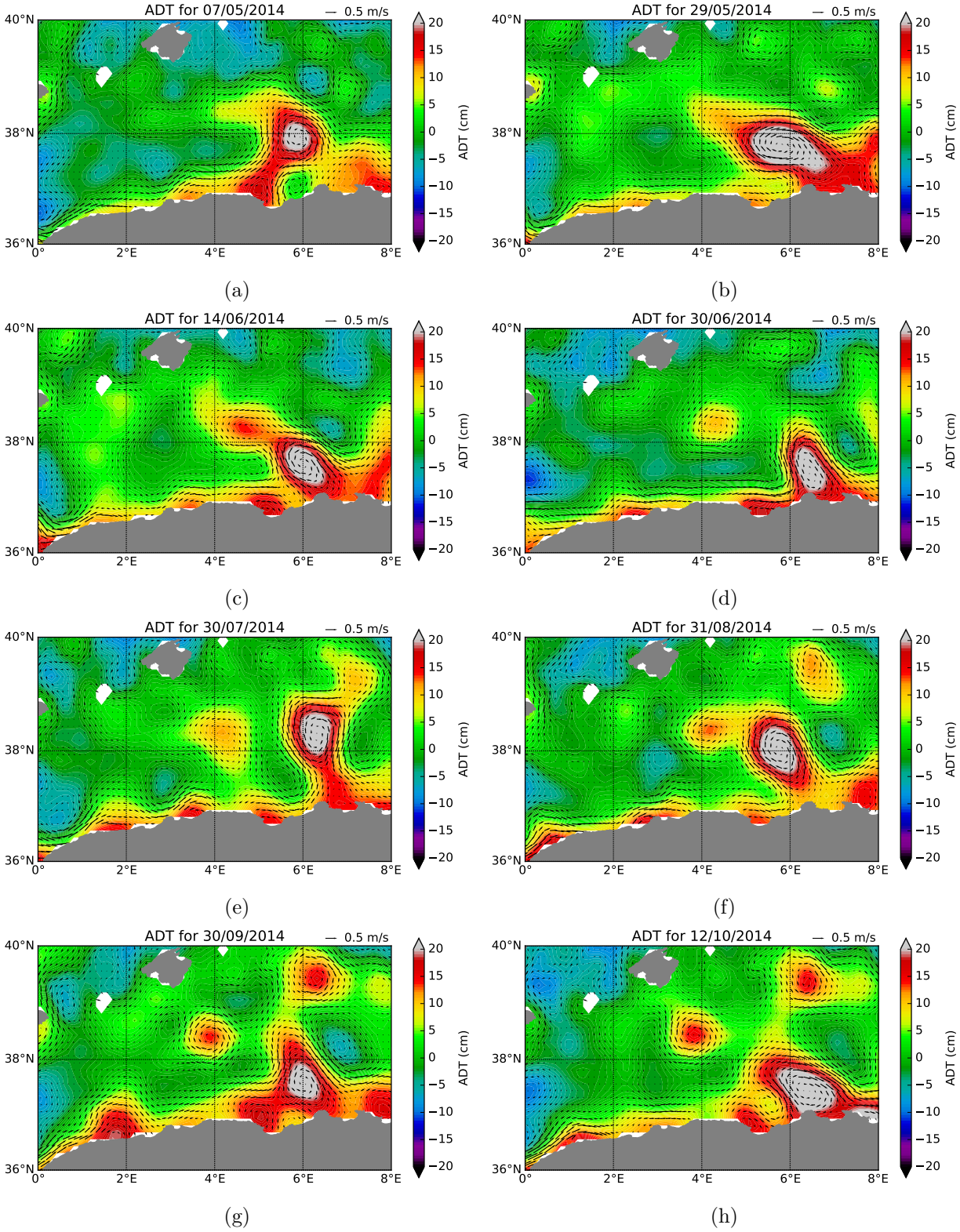

Figure 7: ADT plots with geostrophic velocity on top (vector plot).

3 Methods

3.1 TangPy's code implementation

TangPy's code is based in one of the two models exposed in Tang (1975), which are simple extensions of Eady's (1949) model considering no beta effect. To do so, we use a linearized version of the QG wave equation. The starting point are the frictionless Boussinesq QG vorticity equation (eq. 3a) and the adiabatic equation (eq. 3b),

$$\frac{\partial}{\partial t}\nabla^2\psi + J(\psi, \nabla^2\psi) = f\frac{\partial w}{\partial z}, \tag{3a}$$

$$\frac{\partial}{\partial t}\frac{\partial \psi}{\partial z} + J(\psi, \frac{\partial \psi}{\partial z}) + \frac{N^2}{f}w = 0, \tag{3b}$$

where ψ is the stream function, w the vertical velocity, t the time, f the Coriolis parameter at a reference latitude, N the Brunt-Väisälä frequency, x the distance eastward, y the distance northward and z the distance northward. ∇^2 and J are the Laplacian and Jacobian operator respectively.

Assuming a solution of the form

$$\psi' = Re[\Psi e^{ik(x-ct)}]\sin(ly), \tag{4a}$$

$$w' = Re[We^{ik(x-ct)}]\sin(ly), \tag{4b}$$

where Re denotes 'the real part of', Ψ and W are the complex Fourier coefficients, the wave numbers $k = 2\pi/L$ and $l = \pi/D$ (where L is the wavelength in the x direction and D is the distance between nodal surfaces) and c is the complex phase speed. Substituting these solutions into a linearized version of eq. 3 and combining them to eliminate W leads to

$$\frac{\partial^2\Psi}{\partial^2 z} - (\frac{N\mu}{f})^2\Psi = 0, \tag{5}$$

where $\mu^2 = k^2 + l^2$.

In Tang (1975), two cases are exposed, herein we use the first one, the 2-layer model with a stratified shear layer surmounting a quiescent stratified layer (Fig. 8). The upper layer has a constant shear U/H, where U stands for the basic zonal flow at the top and H for the depth of the layer, whereas the lower layer has no motion and a depth h. The buoyancy frequency (Brunt-Väisälä frequency) has a fixed value for each layer.

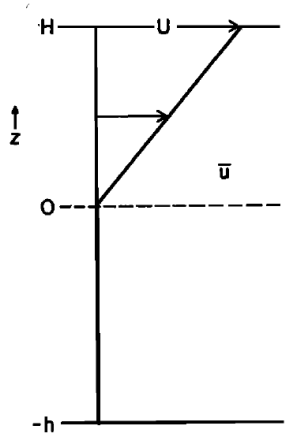

Figure 8: Schematic representation of model used: Layer with constant shear on top of quiescent layer (Tang 1975).

The general solution for introducing a small perturbation (eq. 4), meant to represent a wave of weak amplitude, in the shear layer is

$$\Psi = A\cosh(\xi) + B\sinh(\xi), \tag{6}$$

where

$$\xi = kz/H \quad \text{and} \quad k = \mu HN/f. \tag{7}$$

Considering as boundary conditions that the vertical velocity vanishes at the top and the bottom boundaries and that the flow is continuous across the interface between the layers, we obtain equations for the structure of the unstable waves

$$\psi' = |\Psi|\cos(kX + \theta)e^{\nu t}\sin(ly), \tag{8a}$$
$$w' = |W|\cos(kX - \sigma)e^{\nu t}\sin(ly), \tag{8b}$$

where X and ν (definitions of θ, σ, $|\Psi|$ and $|W|$ can be found on Tang (1975)) are defined as

$$X = x - c_r t, \tag{9a}$$
$$\nu = kc_i, \tag{9b}$$

where c_r and c_i are the real and imaginary phase speeds respectively. For the unstable modes, it must be fulfilled

$$c = c_r + ic_i \quad \text{with} \quad c_i > 0. \tag{10}$$

At this point, before adding all the dynamical expressions, we made a quick verification of the Tang's model, to ensure that the solution for the two layer system was correctly codified (see Appendix A).

From eq. 8a, together with the governing equations for a quasi-geostrophic regime, we can develop the equations for the dynamical processes we want to study (divergence, vorticiy and vertical velocities) on an unstable region. These expressions and their development can be found on the Appendix B.

3.1.1 TangPy parameter selection

Once the model is correctly implemented, the input parameters must be selected by some criteria in order to reproduce an eddy with the properties of an eddy located at the AB. Glider and satellite observations is used to obtain an estimation of these inputs. The adjustable parameters of the model are: the depth of both layers (H and h) (and their corresponding changes in the Brunt-Väisälä frequencies of the layers), the intensity of the zonal flow at the top (U) and the wavelength of the signal (λ).

The geostrophic velocity fields generated from glider data in Cotroneo et al. (2015) can be used to fix the depth of the layers and the zonal flow at the top. These fields (Fig. 9) show that motion layer extents down to 300 m with a maximum intensity of 25 cm s^{-1}. However, previous works on glider data have shown the lack of a barotropic component due to the calculation method (a zero velocity level has to be set as reference). This missing component can be estimated with the depth-average velocity (hereafter DAV). Post mission, the DAV can be used to provide a reference velocity for the geostrophic velocity calculation, providing an estimate of absolute geostrophic velocity (Heslop et al. (2018) and Rodríguez et al. (2017), Fig. 10). This adjustment show that the component not captured in structures like AEs can be of the order of 5 cm s^{-1}. Also, this addition can extent the motion layer down to 500 m. Considering all this, in this work we will use for the depth layers: H = 500 m, $N_1 = 5.8 \cdot 10^{-3}$ s^{-1}, h = 2000 m, $N_2 = 2.3 \cdot 10^{-4}$ s^{-1} and U0 = 0.3 m s^{-1}. The depth of the quiescent layer (h) is the depth from the end of the motion layer to the floor of the basin, so considering a mean depth of the basin of 2500 m and H set to 500 m, the value of h is already obtained. The Brunt-Väisälä frequencies are calculated are obtained from the mean Brunt-Väisälä frequency profile (Fig. 11). This profile is generated from the original density profiles from the glider data through eq. 11,

$$N^2(z) = -\frac{g}{\rho_0}\frac{\partial \rho(z)}{\partial z}, \tag{11}$$

where ρ is the potential density, g is the local acceleration of gravity and z the depth.

The remaining parameter, the wavelength of the signal, can be obtained looking at the spatial dimensions of the AE in the altimetry. The mean diameter of this structure is in the range 112-130 km (Cotroneo et al., 2015), this can be observed at the altimetry plots in Fig. 7. Considering the wavelength is twice the diameter of the eddy, we set a value of 250 km.

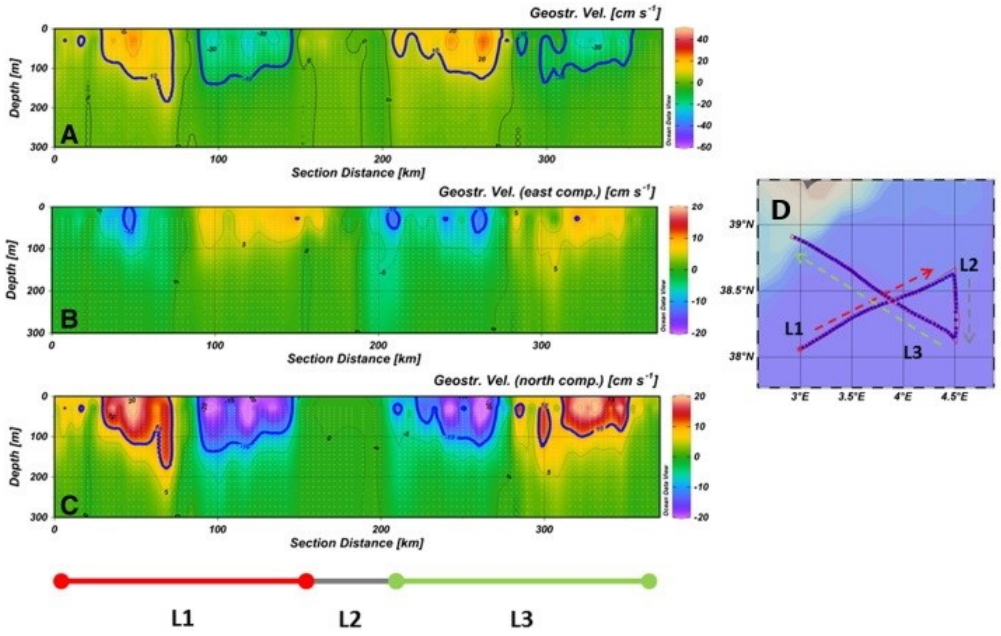

Figure 9: Geostrophic velocity (relative to 850 dbar) calculated from glider CTD data from surface to 300 m depth for the different transects shown (L1, L2 and L3 (d)). (a) Current speed across section. (b) Zonal component. (c) Meridional component. (Cotroneo et al., 2015).

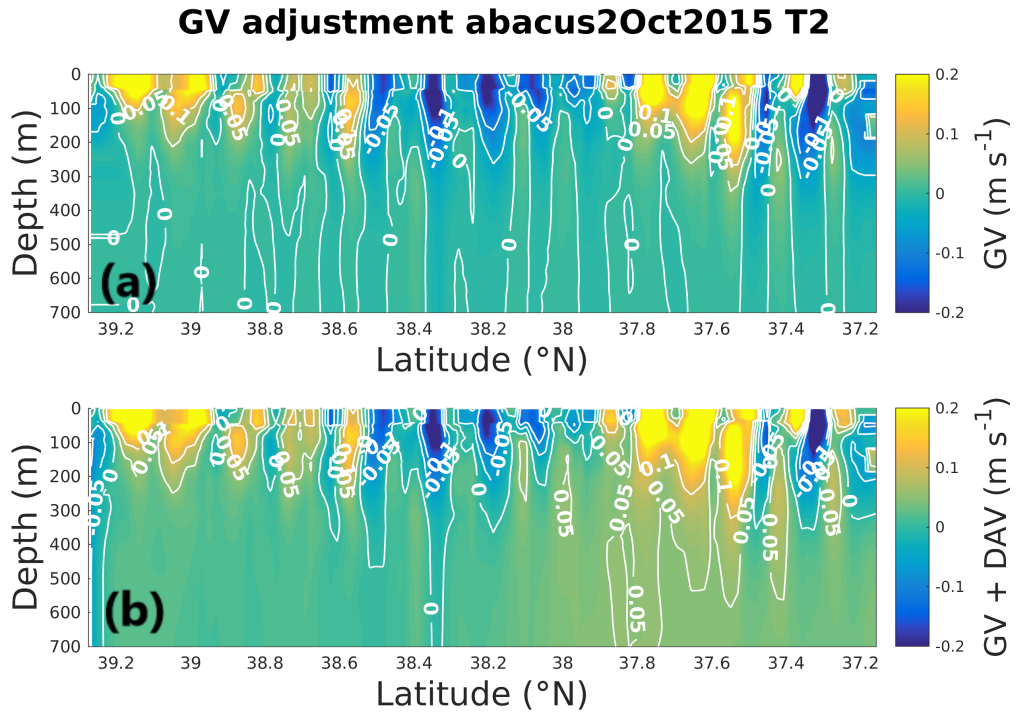

Figure 10: Velocity field across the studied eddy from a transect of ABACUS2. (a) Geostrophic velocity field. (b) DAV adjusted geostrophic velocity field. (Rodríguez et al., 2017)

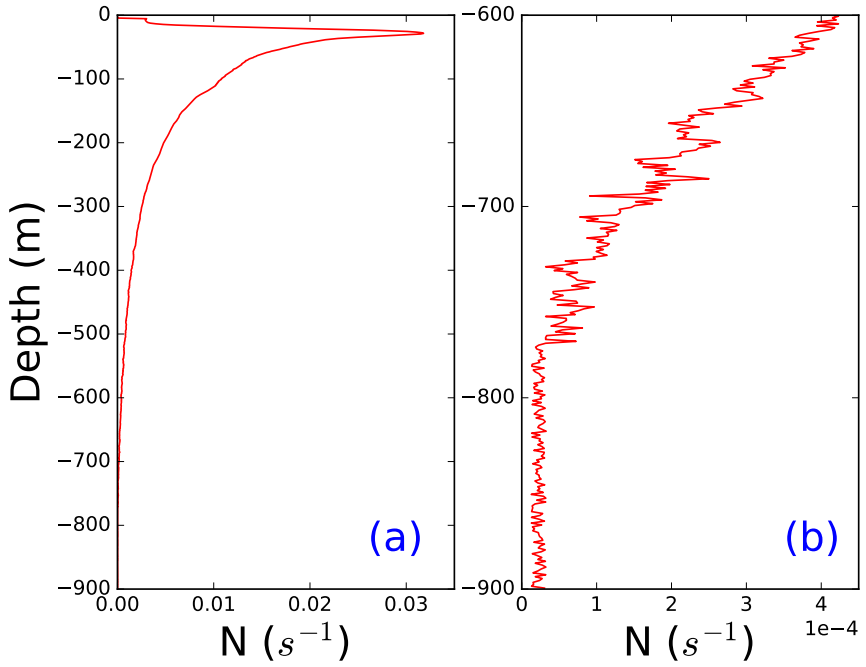

Figure 11: (a) Mean Brunt-Väisälä frequency profile computed from the original density profiles obtained by the glider reaching 900 m. (b) Zoom from (a) in the last 300 m.

3.2 Calculation of divergence using lagrangian observations

The method used here was first introduced by Reed (1971) and studied in Molinari and Kirwan (1975), where the horizontal divergence is estimated from the change in the area of a parcel formed by a set of drifters. However, literature is not vast and there are still many open questions that are being explored in the present (see for example CALYPSO project)

$$div_h \overrightarrow{\mathrm{u}} = A^{-1} \frac{dA}{dt}, \tag{12}$$

The eq. 12 can be proved considering a parcel of side length Δx and Δy, therefore its area will be $A = \Delta x \Delta y$. Considering this, it can be shown

$$A^{-1}\frac{\partial A}{\partial t} = \frac{1}{\Delta x \Delta y}\left(\frac{d(\Delta x \Delta y)}{dt}\right) = \frac{1}{\Delta x \Delta y}\left(\Delta x \frac{d\Delta y}{dt} + \Delta y \frac{d\Delta x}{dt}\right) =$$

$$= \frac{1}{\Delta x}\frac{d\Delta x}{dt} + \frac{1}{\Delta y}\frac{d\Delta y}{dt} = \frac{\partial}{\partial x}\underbrace{\frac{dx}{dt}}_{u} + \frac{\partial}{\partial y}\underbrace{\frac{dy}{dt}}_{v} = \frac{\partial u}{\partial x} + \frac{\partial v}{\partial y} = div_h \overrightarrow{\mathrm{u}}. \tag{13}$$

A minimum of three drifters is required to apply this method even though Molinari and Kirwan (1975) and Okubo and Ebbesmeyer (1976) showed that for an enlarged number of drifters the statistical confidence on the results increases. Despite this, previous studies using triplets of drifters

(Molinari and Kirwan (1975) and Wang et al. (1988)) have obtained significant and consistent results. Following these studies, we use the area rate of change method applied to triplets of drifters.

A common fact in the studies mentioned above is that they use groups of 3 drifters, i.e., they already have the triplets positions. In this work we have a cluster of drifters, therefore we have to design a method/rule to determine how many triplets we can arrange. A scheme of this method is shown in Fig.12. For a given drifter, we check all the possible triplets but keep only those whose the three side distances are lower than a set threshold distance. In this work we have set a threshold distance of 30 km. Just one side of the triplet being greater than the threshold distance is enough to discard this triplet. Looking at drifter C in Fig.12 we obtain two possible triplets, ABC and BCD, but on the second one, the distances $\overline{BD}$ and $\overline{CD}$ are greater than the threshold distance. Hence, the second triplet would not be chosen.

Applying this rule to all the drifters in the cluster we can obtain our triplets of study. It must be noted that when lopping through all the drifters we obtain repeated combinations of drifters (in the example above: $ABC, ACB, BAC, BCA, CAB, CBA$). To avoid it, we design a filter to allow only one combination of the same drifters.

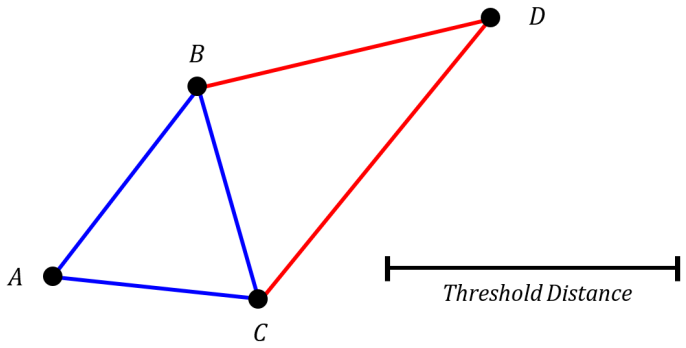

Figure 12: Schematic representation of the triplets selection process.

4 Results

4.1 TangPy results

4.1.1 Baroclinic instability simulation

In this subsection we present the results for the simulations performed with the input parameters selected in section 3.2.1 to reproduce the characteristics of an eddy generated in the AB. For the quoted input parameters, the model gives a propagation speed of 5 km days $^{-1}$ and a doubling time of 12 days. These results can be observed in the Appendix D, where the sequence of growth of the instability for the different dynamical fields is shown. The results shown here correspond to a depth of 50 m. The plot sequence in Fig. 20 in Appendix D shows the dynamic height field (deduced from the stream function ψ, $dh = \psi \cdot f/g$) with the total velocity field on top. It can be seen how the initial instability grows generating a cyclonic circulation followed by an anticyclonic one. This pattern moves eastwards as the instability grows reinforcing the circulation in it until day 6, when a full eddy circulation can be observed. In 10 days, the instability generates a maximum in the dynamic height field of 15 cm and a circulation around of 25 cm/s. This circulation can be decomposed into its geostrophic and ageostrophic components (Fig. 21). As expected based on the QG framework of this work, the ageostrophic field is an order of magnitude smaller than the geostrophic field. Despite this, the ageostrophic field is very relevant in this context as it is the generator of the divergences which develop into vertical movements.

The generation of the convergence and divergence zones generated by the ageostrophic circulation is shown in Fig. 22. This figure show the generation of a divergence zone in front of the anticyclonic gyre while convergence zone is generated behind it. The distribution of the convergence and divergence zones matches with the location of vertical motion. Through continuity, the divergence (convergence) zones develop into ascending (descending) velocities.

Once all the fields of interest are obtained, the next step is to identify at which stage of the analytical simulation the eddy sampled by the glider and drifters is located. Looking back at Fig.7 we can see that the eddy has a dynamic height anomaly around 10 cm, in our simulation this anomaly can be appreciated over the sixth day. Fig. 13 shows all the fields of interest for this date. The model indicates a circulation with velocities around 20 cm/s whose ageostrophic component (around 1 cm/s) generates a divegence maximum around $2.5 \cdot 10^{-3} f$. This divergence translates into a vertical velocity maximum of 28 m/day.

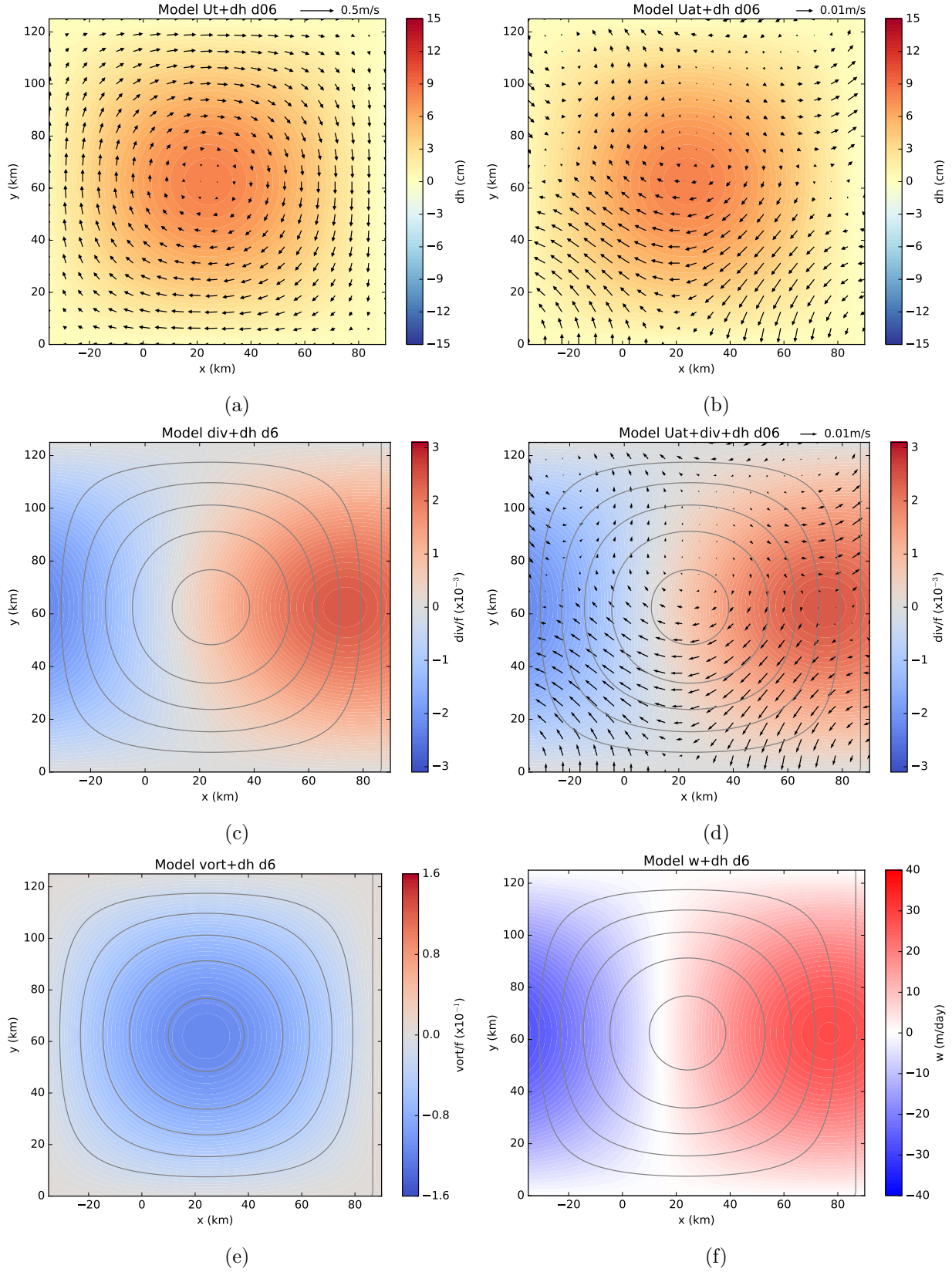

Figure 13: Tang's model results for day 6. (a) Dynamic height with total velocity on top. (b) Dynamic height with ageostrophic velocity on top. (c) Divergence with dynamic height on top. (d) Divergence with dynamic height and ageostrophic velocity on top . (e) Vorticity with dynamic height on top. (f) Vertical velocity with dynamic height on top.

4.1.2 Tang's model sensitivity test

Due to high non-linearity of the expressions inside the TangPy code, it is hard to make an estimation on how each input parameter affects the results. With the objective of gaining perspective on how the input parameters can affect the model output we proceed to do a sensitivity test for the different parameters. The different results obtained by varying H, L and U0 separately are shown in Table 1. The table shows the results for the phase speed, c_r, the time required for the wave to double its amplitude, $T = ln2/\nu$ and the maximum values for the vertical velocity, w, the divergence, div/f and the vorticity, $vort/f$. All the results are for the 4th day simulation since the instability began.

The first results shown are those obtained with different values of H. The total depth of the model remains constant at 2500 m, i.e. if we change H from 500 m to 400 m, h will be 2100 m instead of 2000 m The variation of H also includes the implicit variation of the Brünt-Vaïsala frequency as it depends on the vertical variation of density. Thus, including waters of different depths will modify this variable. The deepening of this layer produces an intensification of the growth of the signal and the vertical velocities but the mean circulation in the gyre lowers down. This effect is represented in an unaltered divergence and a reduced vorticity due to the reduction of the gyre velocity.

The increase in the wavelength results in a reduction of all the magnitudes of the eddy. An expected result, as the same amount of energy, given by the initial instability, is used in a wider area.

The effect of the changes in the zonal flow at the top affects directly at the instability generated. With a greater value of U0, the instability increases as a result of a stronger vertical velocity gradient (vertical shear).

	cr (km/days)	T (days)	Ug (m/s)	w (m/day)	div/f	vort/f
H (m)						
400	4.7	13.3	0.230	23	0.003	0.135
600	5.4	9.9	0.191	28	0.003	0.111
800	6.1	7.4	0.186	33	0.003	0.108
L (km)						
250	5.1	12.2	0.202	25	0.003	0.118
300	4.6	8.9	0.172	17	0.002	0.082
350	4.1	8.7	0.143	11	0.001	0.055
U0 (m/s)						
0,4	6.8	9.2	0.218	36	0.003	0.128
0,6	10.3	6.1	0.253	64	0.006	0.150
0,8	13.7	4.6	0.294	99	0.009	0.176

Table 1: Tang's model sensibility test results for H, L and U0.

4.2 Lagrangian observations

In this section we present the results from the calculations using drifter triplets. Firstly, all the available triplets were considered and we obtained values of divergence around $10^{-1} f$. However, these results showed large changes from day to day and even frequently changed sign. The trajectory of the center of mass of the triplets did not make any sudden jump, in fact they were moving smoothly. To understand these changes, we examined the individual drifter trajectories (see Appendix C). We saw how although the triplet as a whole moved smoothly, the trajectories of the drifters around the center of mass suffered sudden changes. Such a disengage from the main current can be attributed to many factors (small-scale flow and turbulence) and will be discussed later (see section 5.2). such behavior got accentuated forward in time, even some drifters got advected away, not only from the eddy but even from the region.

The triangle method used by Molinari and Kirwan (1975) was proven not to get good results for those triangles where the drifters were too far from the center. Therefore, we decided not to use the drifters that suffered sudden jumps in their trajectory. After applying this condition, there were only three drifters which did not suffer sudden changes and remained in the eddy circulation. This supposes a great limitation to our results, as we only have one triplet available and therefore any comparison between triplets is discarded. Nevertheless, the application of this condition is of utmost importance for the proper functioning of the method. The trajectories for the first 20 days of analysis of the three drifters are shown in Fig. 14 together with the ADT of the 25th of May (when the drifters where at the middle of the trajectory plotted) showing the correspondence between the drifters trajectory and the eddy circulation.

As we can see in Fig. 14, the movement of the drifters have an important component due to the inertial oscillation. These characteristic movement due to Coriolis will only add noise to the evolution of the triplet area; hence we will apply a time filter of 36 h (twice the period of the signal, which at a latitude of 40º is around 17.5 h) in order to remove this signal.

The divergence results for the filtered trajectories are shown in Fig. 15. In this sequence of plots we can see the evolution of the triplet together with the value of divergence located at the center of mass for each time. Fig. 15f shows the divergence estimates at all time. Note that there are two periods of time where we start to get large values of convergence followed by a sudden change in sign, obtaining large values of divergence. These high values are caused by the shape of the triangle as it is no longer isotropic. This happens when the triangle gets too elongated and therefore the method used, as stated by Molinari and Kirwan (1975) no longer gives correct estimates until the triangle gets an isotropic shape again. In general terms, we obtain consitent and reasonable values for a mesoscale eddy around 0.1 f - 0.3 f for a mesoscale eddy.

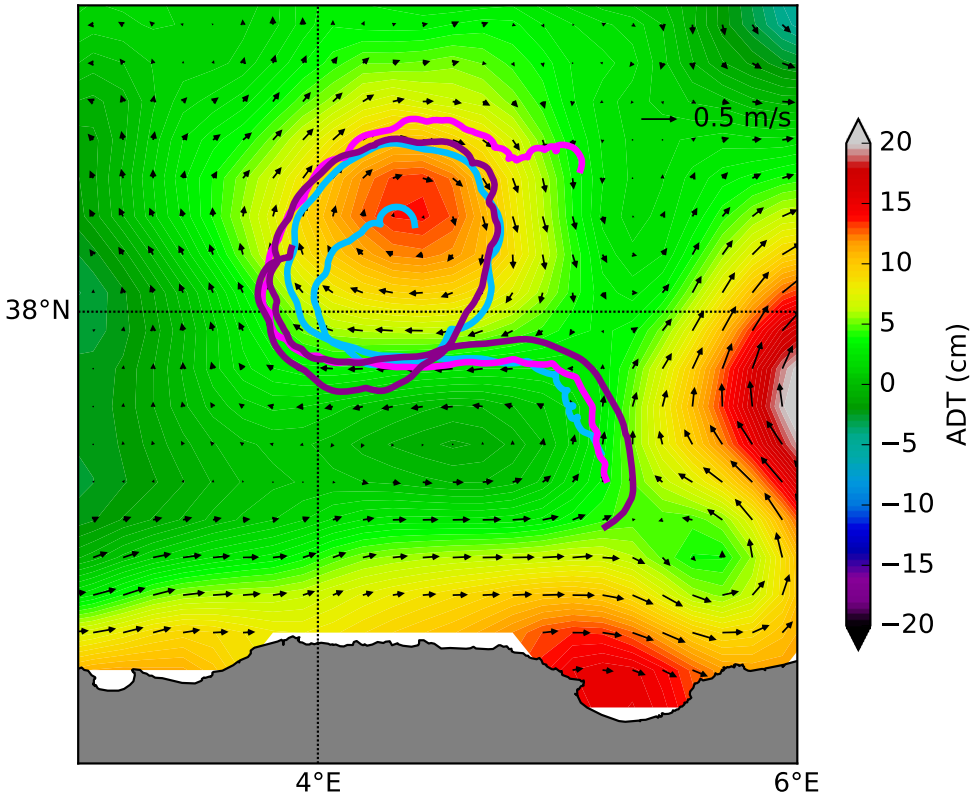

(a)

Figure 14: Trajectory of the first 20 days of analysis of the drifters which stayed in the eddy circulation together with the ADT for the 25th of May, when the drifters where at the middle of the trajectory plotted (filled contour) with the estimated geostrophic velocity field on top (vector plot).

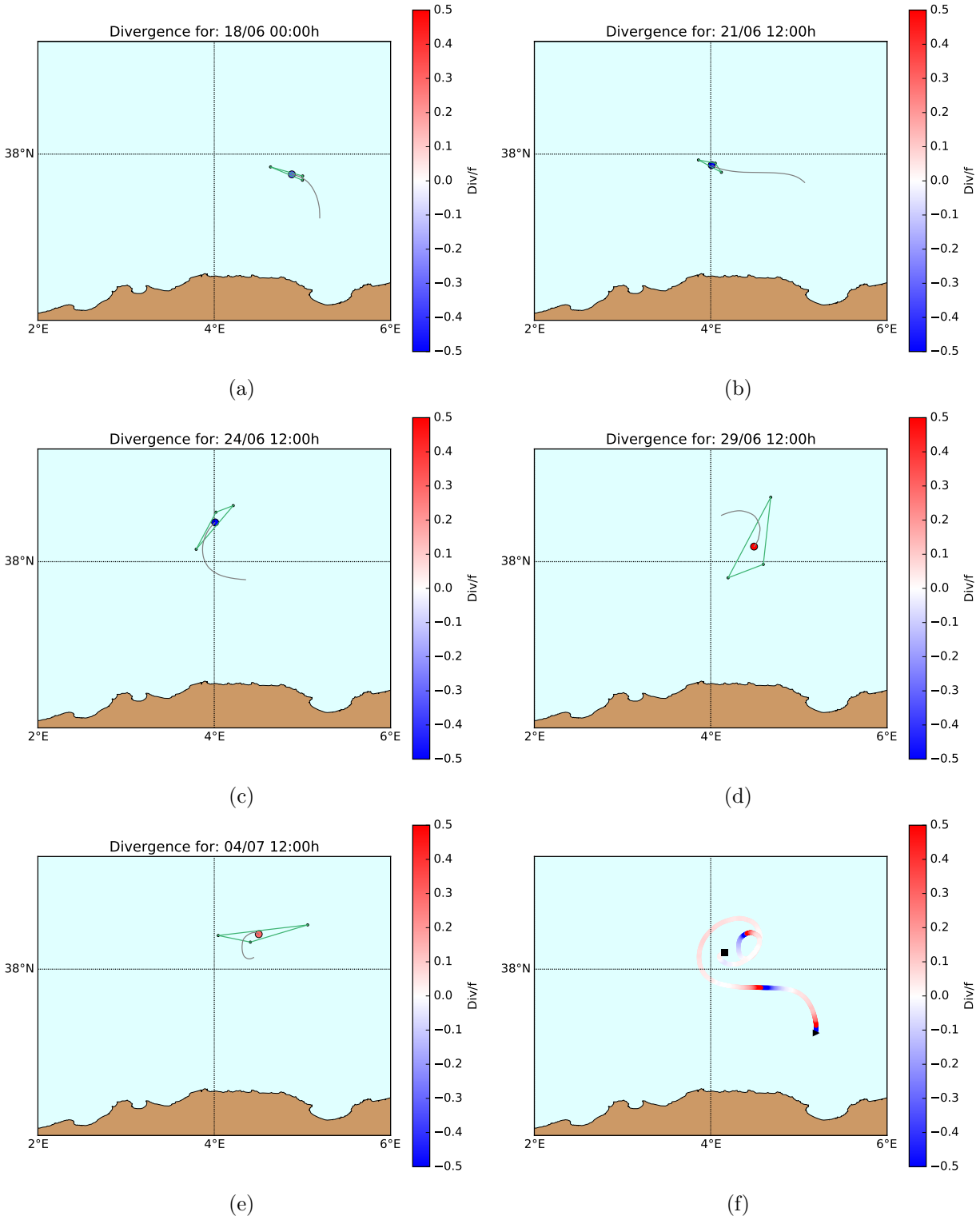

Figure 15: Evolution of the triplet of study and the divergence estimate at the center of mass of the triplet (a)-(e). Divergence estimate at each point of the trajectory (f).

5 Discussion

5.1 Glider results comparison

In order to analyze the capability of the analytical model of Tang to describe structures such as the ones studied in this work, we compared the QG vertical velocity (w-QG , hereafter) field calculated from the model with the velocity field derived from glider data across the eddy (Fig. 16). Cotroneo et al. (2015) finds out a region of upward motion in the eastern part of the domain while a region of downward motion is located at the western side of the eddy. This distribution is recreated by the Tang model for the anicyclonic gyre too (Fig. 16a). Thus there is a match in the location of the regions of vertical motion between the model and the calculated field from observations although there is a difference in the magnitudes of both fields. First, the model predicts stronger vertical velocities than the calculated ones, but this difference possibly comes from the lack of observations in the calculation of the w-QG. It should be noted that, with the domain considered, only 2 transects of data across the eddy are available (16b). Therefore it is necessary to carry out a strong interpolation of the results, which can cause a softening of the original signal and therefore obtain vertical motions of less intensity than the predicted by the model. Also, it is remarkable that the model shows a symmetry at both sides of the eddy (same intensity but opposed sign) but in the calculated field, the downward motions at the west are an order of magnitude bigger than the upward motions at the east. This could be caused by the spatial distribution of the observations, missing the region of stronger upward motions. Another explanation for this difference can be due to the fact that the model is generating the w-QG field only as a product of a baroclinic instability, hence not taking into account all of the other geophysical factors and small scale flows that can affect such a circulation.

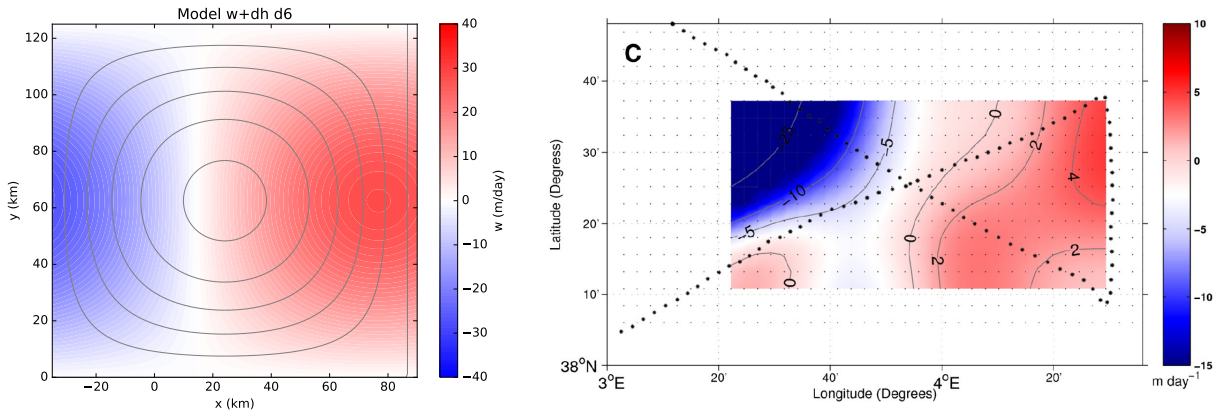

(a) (b)

Figure 16: (a) Vertical velocity field from Tang's analytical model. (b) Vertical velocity field derived from glider data across the eddy (black dots) from Cotroneo et al. (2015).

5.2 Difference between the two methods

From the results of the two methodologies used in this work, the difference in order of magnitude obtained between both methods stands out. We obtain two orders of magnitude between the Eulerian divergence (calculated from TangPy) and the Lagrangian divergence (calculated from triplets of drifters). This difference can be explained by the nature of each method. However this difference also could be emerging from a calculation error. To make sure this is not the origin of the difference we compared both results with previous studies to check their consistency.

The w-QG results from TangPy have already been discussed in the previous section and proven to reproduce the field correctly. Making use of eq. 1, we can use the w-QG fields from TangPy to calculate through finite differences the divergence field at the mid level. The divergence field at 50 m depth was calculated using three different depth layers. For the three intervals we obtained a divergence of the same order of the analytical divergence field maximum. Therefore, this result is consistent with the w-QG fields.

Regarding the results from the drifters, we have compared them with the Lagrangian divergences obtained in previous studies (Reed, 1971; Molinari and Kirwan, 1975; Wang et al., 1988; Poulain, 1992; LaCasce and Ohlmann (2003)). Taking into account the variation of the results as these studies take place in different regions, all of them agree in the magnitude order with our results, obtaining values between 0.1 f and 0.5 f. Besides this, we can assume that our results may incorporate variations due to the high distance between drifters.

Therefore, both methods show consistent results. The difference in magnitude between both methods. TangPy is generating an analytical field taking into account only QG while the drifters are capturing the whole signal of the velocity at surface (15 m). In the last two decades, a wide range of studies have focused on the behaviour of the dispersion of drifters (LaCasce and Ohlman, 2003; LaCasce, 2008; Beron and LaCasce, 2016; Berta et al., 2016) and its effect on the Lagrangian fields (Kalda et al., 2014; Hernandez-Carrasco et al., 2018). These studies show an extremely complicated relation between the surface velocities and the Lagrangian divergence. Mesoscale and basin-scale properties of the surface velocities exhibit much lower 3D effects compared with realistic flows in marine environment (Kalda et al., 2014). LaCasce and Ohlman (2003) dealt with similar problems and found that the surface Ekman flow and also the effect of windage were factors that could affect and defflect the drifters from the main current.

6 Conclusion

In this master's thesis we have analyzed a mesoscale eddy using two different methods, obtaining consistent results with previous studies. Firstly, we have been able to develop a Python code based on Tang's model to simulate the circulation generated by a baroclinic instability and the dynamic fields of interest associated to it. Despite being a simplified QG model, the simulations obtained show a good match with the observations and the calculated fields inferred from glider data observations. This fact shows the big advantages of running this cheap and fast model in terms of computational cost against other numerical models commonly used as WMOPS or CMEMS among others. Secondly, we have implemented the method of triangles to calculate the rate of change of a triplet of drifters. This method has not shown as good results as the previous one. Nevertheless, the results are consistent with results from previous studies that have used this method. To obtain a better description of the divergence field a larger and closer cluster of drifters would have been needed. Considering this, this is a method with room for improvement that can be useful in the detection of convergence or divergence zones from the drift of particles on surface.

These results have allowed us the observation of the dependency of the results on the approach taken to calculate them. Lagrangian results from drifters result in a higher intensity signal than the Eulerian results from the model, as the first ones capture the whole signal on surface. Moreover, drifters have proven to be an excellent method of observation of mesoscale convergence and divergence zones. Therefore the development and understanding of the techniques used to obtain estimates of convergence and divergence is crucial. The method used here is not the only one that exists and the next objective is to study and implement alternative methods (see next section).

Finally, it is worth mentioning the use of observations from different platforms in this work. Multiplatform observations provide an independent and full description of the structure studied, allowing the user to make use of the advantages of each platform.

7 Further work

During this work a set of questions or ideas have arised which, due to time reasons, have not been answered. These items prescribe a line for future work in order to improve the results obtained and gain more information about the dynamics of convergence and divergence zones. The principal subjects to continue working are the following ones.

7.1 Alternative methods for the calculation of divergence zones from Lagrangian observations

Molinari and Kirwan (1975) study two methods of calculating convergence or divergence zones from drifters trajectories. In this work we have studied and applied the first one, based on the rate of change of the area formed by a triplet of drifters. The second one is called the *Least Squares method* based on expanding the velocities of the individual drifters in Taylor series about the velocity of the cluster center (eq. 14),

$$u_i = u_c + \frac{\partial u_c}{\partial x}(x_i - x_c) + \frac{\partial u_c}{\partial y}(y_i - y_c) + u_i\prime, \tag{14a}$$

$$v_i = u_c + \frac{\partial v_c}{\partial x}(x_i - x_c) + \frac{\partial v_c}{\partial y}(y_i - y_c) + v_i\prime, \tag{14b}$$

where (x_c, y_c) and (u_c, v_c) are the positions and velocities of the cluster center and (x_i, y_i) and (u_i, v_i) are the positions and velocities of the drifters. However, to use this method the cluster has to be small enough so that the shears are locally linear (as we retain only the first order term of the Taylor expansion). These equations can be used to estimate the divergence and vorticity using a least squares formulation. This method allows the estimation of errors for the values if four or more drifters are used.

Another method has been used in the calculation of divergence zones. D'Asaro et al, (2017) estimates divergence from the drifter trajectories using a central difference of the positions and considering an ellipse. The center of the ellipse is set by the mean position of the drifters in the cluster and the semiaxis are defined as the variance in position of the cluster. By evaluating the change of the area of the ellipse, an estimation of the divergence can be obtained. These estimates are more accurate if the drifter cluster is roughly isotropic, as happened with the triangle method.

7.2 Simulation of Lagrangian trajectories over TangPy's output

It would be interesting to see the results obtained from merging both methods. This possibility appears by using a Lagrangian trajectory model called TracPy based on the TRACMASS algorithm (Thyng and Hetland, 2014). TracPy can run a simulation of Lagrangian trajectories of virtual drifters given a velocity field. Thus, by giving as input the velocity fields obtained from TangPy, we can generate a cluster of virtual drifters and then apply the triangle method. This would allow us to compare the divergences obtained from the virtual drifters with those obtained from the model. As these drifters only are influenced by the QG field (they are not influenced by any small-scale flow or turbulence), both results should match if the method of drifters is consistent.

7.3 CALYPSO project

CALYPSO (Coherent Lagrangian Pathways from the Surface Ocean to Interior) is a research iniciative of the Office of Naval Research (ONR) with the participation of international oceanographic research centers as Woods Hole Oceanographic Institution (WHOI), SCRIPPS institution of oceanography, University of Washington and Instituto Mediterraneo de Estudios Avanzados (IMEDEA). The aim of this project is to answer some of the question that were stated on the motivation section of this work: Establish an understanding and predictive ability of the 3D coherent pathways from surface to the interior, implement observational study to test the current theories about these pathways and also improve the capability with the models.

This study will take place in the Southwest Mediterranean Sea (Alboran Sea), a region with strong and unstable fronts between Mediterranean salty waters and the relatively fresh Atlantic water. Therefore strong zones of convergence and subsidence can be found, which makes it a perfect place to test all the theories. A pilot mission took place the last May 2018 to get a first contact with the region. In this pilot mission five different types of surface drifters were deployed (a total amount of 70 drifters) together with a 3D Lagrangian float (D'Asaro et al., 2017). Meanwhile, the front was sampled with UCTD and CTD casts combined with three gliders.

Figure 17: Scientific staff from the CALYPSO pilot mission. NRV Alliance on the background.

Acknowledgments

Lo primero de todo, me gustaría agradecer a mi tutora Ananda toda la confianza y seguridad que me ha transmitió cuando me propuso este trabajo. A pesar del reto que suponía comenzar con una nueva línea de investigación, no dude ni un segundo ya que sabía que iba a estar perfectamente guiado. Miro atrás y me impresiona la cantidad de conocimiento que he adquirido en este año, muchas gracias. Luego me gustaría también, agradecer a Simón, Evan, Antonio y Bárbara todo lo que me han ayudado. Siempre que he acudido a ellos con alguna duda me la han resuelto sin ningún problema.

Después, también me gustaría mencionar al grupo de meteo de la UIB, especialmente a los miembros del lab. A pesar de que ya no forme parte del grupo me han tratado como si lo fuese y siempre han estado allí cuando los he necesitado. Sin ellos este trabajo tampoco podría haber salido hacia delante.

Finalmente, pero no menos, agradecer a mis compañeros del Máster, Aina y Toni. Entre los tres hemos conseguido crear un equipo imparable y habéis hecho que el Máster se me haya pasado volando. Toni, eres un crack y un currante y conseguirás cosas geniales. Tu Aina..., no tengo palabras para ti...eres demasiado. Nuestros caminos ahora tocan separarse, y a pesar de que puede parecer algo malo, a mí me ilusiona ya que sé que nos mantendremos en contacto y podremos contarnos todos los avances que vamos haciendo en nuestros respectivos campos, que estoy seguro que por lo menos por vuestra parte, no serán pocos.

Por último, ahora ya sí, dar las gracias a todas aquellas personas que me han apoyado y ayudado durante este trabajo: compañeros de la uni, compañeros del SOCIB, amigos... muchas gracias.

Bibliography

[1] J. T. Allen, D. A. Smeed, A. J.G. Nurser, J. W. Zhang, and M. Rixen. Diagnosis of vertical velocities with the QG omega equation: An examination of the errors due to sampling strategy. *Deep-Sea Research Part I: Oceanographic Research Papers*, 48(2):315–346, 2001.

[2] J.T. Allen, S.C. Painter, and M. Rixen. Eddy transport of Western Mediterranean Intermediate Water to the Alboran Sea. *J. Geophys. Res.*, 113(March):1–17, 2008.

[3] F. J. Beron-Vera and J. H. LaCasce. Statistics of simulated and observed pair separations in the Gulf of Mexico. *Amer. Meteor. Soc.*, pages 2183–2199, 2016.

[4] M Berta, A Griffa, T M. Özgökmen, and A C. Poje. Submesoscale evolution of surface drifter triads in the Gulf of Mexico. *Geophys. Res. Lett.*, 43(22):11,751–11,759, 2016.

[5] M Berta, A Griffa, T M. Özgökmen, and A C. Poje. Submesoscale evolution of surface drifter triads in the Gulf of Mexico. *Geophys. Res. Lett.*, 43(22):11,751–11,759, 2016.

[6] B. Buongiorno Nardelli, S. Guinehut, A. Pascual, Y. Drillet, S. Ruiz, and S. Mulet. Towards high resolution mapping of 3-D mesoscale dynamics from observations. *Ocean Science*, 8(5):885–901, 2012.

[7] Y Cotroneo, G Aulicino, S Ruiz, A Pascual, G Budillon, G Fusco, and J Tintoré. Glider and satellite high resolution monitoring of a mesoscale eddy in the algerian basin: Effects on the mixed layer depth and biochemistry. *J. Mar. Syst.*, 162:73–88, 2015.

[8] Benoit Cushman-Roisin and Jean-Marie Beckers. *Introduction to geophysical fluid dynamics: physical and numerical aspects*, volume 101. Academic press, 2011.

[9] E A. D'Asaro, A Y. Shcherbina, J M. Klymak, J Molemaker, G Novelli, C M. Guigand, A C. Haza, B K. Haus, E H. Ryan, G A. Jacobs, H S. Huntley, N J. M. Laxague, S Chen, F Judt, J C. McWilliams, R Barkan, A. D. Kirwan, A C. Poje, and T M. Özgökmen. Ocean convergence and the dispersion of flotsam. *Proc. Nat. Acad. Sci.*, page 201718453, 2018.

[10] E. T. Eady. Long Waves and Cyclone Waves. *Tellus*, 1(3):33–52, 1949.

[11] R. Escudier, B. Mourre, M. Juza, and J. Tintoré. Subsurface circulation and mesoscale variability in the Algerian subbasin fromaltimeter-derived eddy trajectories. *J. Geophys. Res. Oceans*, 121:5452–5469, 2016.

[12] M. M. Flexas, X. Durrieu de Madron, M. A. Garcia, M. Canals, and P. Arnau. Flow variability in the Gulf of Lions during the MATER HFF experiment (March-May 1997). *J. Mar. Syst.*, 33-34(May 1997):197–214, 2001.

[13] D Gomis, A Pascual, and M A. Pedder. Errors in dynamical fields inferred from oceanographic cruise data: Part II. The impact of the lack of synopticity. *J. Mar. Syst.*, 56(3-4):334–351, 2005.

[14] I Hernández-Carrasco, A Orfila, V Rossi, and V Garçon. Effect of small scale transport processes on phytoplankton distribution in coastal seas. *Sci. Rep.*, (May):1–13, 2018.

[15] E. E. Heslop, A. Sánchez-Román, A. Pascual, D. Rodríguez, K. A. Reeve, Y. Faugère, and M. Raynal. Sentinel-3A Views Ocean Variability More Accurately at Finer Resolution. *Geophys. Res. Lett.*, 44(24):12,367–12,374, 2018.

[16] J Kalda, T Soomere, and A Giudici. On the finite-time compressibility of the surface currents in the Gulf of Finland, the Baltic Sea. *J. Mar. Syst.*, 129:56–65, 2014.

[17] Pijush K Kundu, Ira M Cohen, and DW Dowling. Fluid mechanics 4th, 2008.

[18] J. H. LaCasce. Statistics from Lagrangian observations. *Prog. Oceanogr.*, 77(1):1–29, 2008.

[19] J. H. LaCasce and Carter Ohlmann. Relative dispersion at the surface of the Gulf of Mexico. *J. Mar. Res.*, 61(3):285–312, 2003.

[20] A Mahadevan and A Tandon. An analysis of mechanisms for submesoscale vertical motion at ocean fronts. *Ocean Modelling*, 14(3-4):241–256, 2006.

[21] C Millot. Circulation in the Western Mediterranean Sea. *J. Mar. Syst.*, 20(1-4):423–442, 1999.

[22] C. Millot and I. Taupier-Letage. Additional evidence of LIW entrainment across the Algerian subbasin by mesoscale eddies and not by a permanent westward flow. *Prog. Oceanogr.*, 66(2-4):231–250, 2005.

[23] R. Molinari and A. D. Kirwan. Calculations of Differential Kinematic Properties from Lagrangian Observations in the Western Caribbean Sea, 1975.

[24] PP Niiler, JD Paduan, AL Sybrandy, and L Bombardier. The woce/toga lagrangian surface drifter. In *OCEANS'91. Ocean Technologies and Opportunities in the Pacific for the 90's. Proceedings.*, volume 2, pages 839–843. IEEE, 1991.

[25] P P. Niller, P Poulain, and L R. Haury. Synoptic three-dimensional circulation in an onshore-flowing filament of the California Current. *Deep Sea Research Part A, Oceanographic Research Papers*, 36(3), 1989.

[26] A Okubo, C C Ebbesmeyer, and J M Helseth. Determination of Lagrangian Deformations from Analysis of Current Followers, 2010.

[27] A Okubo, C C. Ebbesmeyer, and B G. Sanderson. Lagrangian diffusion equation and its application to oceanic dispersion. *J. Oceanogr. Soc. Japan*, 39(5):259–266, 1983.

[28] A Pascual, D Gomis, R L. Haney, and S Ruiz. A Quasigeostrophic Analysis of a Meander in the Palamós Canyon: Vertical Velocity, Geopotential Tendency, and a Relocation Technique. *J. Phys. Oceanogr.*, 34(10):2274–2287, 2004.

[29] A Pascual, S Ruiz, B Buongiorno Nardelli, S Guinehut, D Iudicone, and J Tintoré. Net primary production in the Gulf Stream sustained by quasi-geostrophic vertical exchanges. *Geophys. Res. Lett.*, 42(2):441–449, 2015.

[30] A Pascual, S Ruiz, A Olita, C Troupin, M Claret, B Casas, B Mourre, P-M Poulain, A Tovar-Sanchez, A Capet, E Mason, J T. Allen, A Mahadevan, and J Tintoré. A Multiplatform Experiment to Unravel Meso- and Submesoscale Processes in an Intense Front (AlborEx). *Front. Mar. Sci.*, 4(February):1–16, 2017.

[31] A. C. Poje, T. M. Ozgokmen, B. L. Lipphardt, B. K. Haus, E. H. Ryan, A. C. Haza, G. A. Jacobs, A. J. H. M. Reniers, M. J. Olascoaga, G. Novelli, A. Griffa, F. J. Beron-Vera, S. S. Chen, E. Coelho, P. J. Hogan, A. D. Kirwan, H. S. Huntley, and A. J. Mariano. Submesoscale dispersion in the vicinity of the Deepwater Horizon spill. *Proc. Nat. Acad. Sci.*, 111(35):12693–12698, 2014.

[32] P-M Poulain. Estimates of Horizontal Divergence and Vertical Velocity in the Equatorial Pacific, 1993.

[33] R. K. Reed. An Observation of Divergence in the Alaskan Stream. *J. Phys. Oceanogr.*, 1(4):282–283, 1971.

[34] D Rodríguez, E Heslop, J Allen, J Tintoré, B Mourre, Y Cotroneo, G Aulicino, A Pascual, and S Ruiz. Algerian Basin Glider Results. *SOCIB internal report*, 2017.

[35] S. Ruiz, J. Font, M. Emelianov, J. Isern-Fontanet, C. Millot, J. Salas, and I. Taupier-Letage. Deep structure of an open sea eddy in the Algerian Basin. *J. Mar. Syst.*, 33-34:179–195, 2002.

[36] J Salas, C Millot, J Font, and E García-Ladona. Analysis of mesoscale phenomena in the Algerian basin observed with drifting buoys and infrared images. *Deep-Sea Research Part I: Oceanographic Research Papers*, 49(2):245–266, 2001.

[37] C. Sammari, C. Millot, and L. Prieur. Aspects of the seasonal and mesoscale variabilities of the Northern Current in the western Mediterranean Sea inferred from the PROLIG-2 and PROS-6 experiments. *Deep-Sea Research Part I*, 42(6):893–917, 1994.

[38] C Tang. Baroclinic Instability of Stratified Shear Flows in the Ocean and Atmosphere. *J. Geophys. Res.*, 80(9):1168–1175, 1975.

[39] P. Testor, U. Send, J. C. Gascard, C. Millot, I. Taupier-Letage, and K. Béranger. The mean circulation of the southwestern Mediterranean Sea: Algerian Gyres. *J. Geophys. Res. Oceans*, 110(11):1–14, 2005.

[40] K M Thyng and R D Hetland. TracPy : Wrapping the Fortran Lagrangian trajectory model TRACMASS. *Proc. of the 13th Python in Science Conf. (Scipy 2014)*, (Scipy):85–90, 2014.

[41] J Tintoré, D Gomis, S Alonso, and G Parrilla. Mesoscale Dynamics and Vertical Motion in the Alborán Sea, 1991.

[42] D-P Wang, M E. C. Vieira, J Salat, J Tintoré, and P E. La Violette. A shelf/slope frontal filament off the northeast Spanish Coast. *J. Mar. Res.*, 46(2):321–332, 1988.

Appendix A

Because of the complexity and length of the algorithm that implements the Tang's model we proceed to do a verification comparing our results with the results shown in Tang (1975). There, a simple simulation is performed to obtain baroclinic waves in the ocean (Table 2).

h/H	κ	L, **km**	c_r, **cm s**$^{-1}$	ν, **10**$^{-6}$ **s**$^{-1}$	T, **days**
1	1,10*	427	17.6	1.926	4.17
2	1.05*	447	14.4	1.604	5.00
3	1.00*	469	12.9	1.443	5.56
3	0.80	587	11.3	1.353	5.93
3	0.40	1174	8.6	0.798	10.05

Table 2: Parameters and solutions for Baroclinic waves in Ocean. Values of κ with * represent the most unstable wave.

We will generate the same output variables as Tang's to check the code developed in this work. The checked variables are the phase speed, c_r, the growth rate, ν and the time required for the wave to double its amplitude, $T = ln2/\nu$. The parameters considered for this simulation are $f = 0.898 \cdot 10^{-4} s^{-1}$ (latitude of 38°), $D = L = 427\,km$, $N_1 = 6 \cdot 10^{-3} s^{-1}$, $N_2 = 2 \cdot 10^{-3} s^{-1}$, $h = H = 1\,km$ and $U0 = 60\,cm^{-1}$.

The results obtained from the simulation with these parameters match perfecctly with those in Tang (1975).

$$
\begin{aligned}
c_r &= 15.2\,km/day\,(17.6\,cm/s) \\
\nu &= 1.93 \cdot 10^{-6}\,s^{-1} \\
T &= 4.17\,days
\end{aligned}
$$

Appendix B

We will work with the equations of motion with the following assumptions:

- $\rho = \overline{\rho}(z) + rho'(x, y, z, t) \qquad |\rho'| \ll |\overline{\rho}|$
- $p = \overline{p} + p'(x, y, z, t)$
- Beta plane: $f = f_0 + \beta y$
- No friction

With these assumptions, the horizontal momentum equations will be:

$$\frac{du}{dt} - f_0 v - \beta_0 y v = -\frac{1}{\rho_0}\frac{\partial p'}{\partial x}, \tag{15a}$$

$$\frac{dv}{dt} - f_0 u - \beta_0 y u = -\frac{1}{\rho_0}\frac{\partial p'}{\partial y}. \tag{15b}$$

Where the operator $\frac{d}{dt}$ stands for the substantial derivative:

$$\frac{d}{dt} = \frac{\partial}{\partial t} + u \cdot \nabla. \tag{16}$$

To obtain vertical velocities, we have to include a small ageostrophy correction, this is equivalent to say we are working on the quasi-geostrophy theory,

$$u = u_g + u_a, \tag{17a}$$

$$v = v_g + v_a. \tag{17b}$$

Here, we will try to find an expression in terms of the stream function ψ for the eq. 15 . To do so, we will substitute the velocities present at eq. 15 for their respective geostrophic expressions,

$$u_g = -\frac{1}{f_0\rho_0}\frac{\partial p'}{\partial y}, \tag{18a}$$

$$v_g = \frac{1}{f_0\rho_0}\frac{\partial p'}{\partial x}, \tag{18b}$$

also, we have to consider the substantial derivative as

$$\frac{d_g}{dt} = \frac{\partial}{\partial t} + u_g \cdot \nabla_h. \tag{19}$$

With all these assumptions, for the x dimension we have,

$$\partial_t u_g + u_g \cdot \partial_x u_g + v_g \partial_y u_g - f_0 v - \beta_0 y v_g = -\frac{1}{\rho_0}\frac{\partial p'}{\partial x}, \tag{20}$$

substituting the expressions from eq. 18,

$$-\frac{1}{\rho_0} f_0 \frac{\partial^2 p'}{\partial t \partial y} + \frac{1}{\rho_0^2 f_0^2}\frac{\partial p'}{\partial y}\frac{\partial^2 p'}{\partial x \partial y} - \frac{1}{\rho_0^2 f_0^2}\frac{\partial p'}{\partial x}\frac{\partial^2 p'}{\partial^2 y} - f_0 v - \frac{\beta_0}{\rho_0 f_0} y \frac{\partial p'}{\partial x} = -\frac{1}{\rho_0}\frac{\partial p'}{\partial x}, \tag{21}$$

where the 2nd and 3rd term can be identified as the result of the Jacobian (eq. 22),

$$J(a,b) = \frac{\partial a}{\partial x}\frac{\partial b}{\partial y} - \frac{\partial a}{\partial y}\frac{\partial b}{\partial x}, \tag{22}$$

therefore eq. 21 can be rewritten as,

$$-\frac{1}{\rho_0} f_0 \frac{\partial^2 p'}{\partial t \partial y} - \frac{1}{\rho_0^2 f_0^2} J(p', \frac{\partial p'}{\partial y}) - f_0 v - \frac{\beta_0}{\rho_0 f_0} y \frac{\partial p'}{\partial x} = -\frac{1}{\rho_0}\frac{\partial p'}{\partial x}. \tag{23}$$

Identically, the same goes for the y dimension,

$$\frac{1}{\rho_0} f_0 \frac{\partial^2 p'}{\partial t \partial x} + \frac{1}{\rho_0^2 f_0^2} J(p', \frac{\partial p'}{\partial x}) + f_0 u - \frac{\beta_0}{\rho_0 f_0} y \frac{\partial p'}{\partial y} = -\frac{1}{\rho_0}\frac{\partial p'}{\partial y}. \tag{24}$$

From eq. 23 and eq. 24 it is immediate to isolate an expression for both u and v,

$$u = -\frac{1}{\rho_0 f_0}\frac{\partial p'}{\partial y} - \frac{1}{\rho_0 f_0^2}\frac{\partial^2 p'}{\partial t \partial x} - \frac{1}{\rho_0^2 f_0^3} J(p', \frac{\partial p'}{\partial x}) + \frac{\beta_0}{\rho_0 f_0^2} y \frac{\partial p'}{\partial y}, \tag{25a}$$

$$v = \frac{1}{\rho_0 f_0}\frac{\partial p'}{\partial x} - \frac{1}{\rho_0 f_0^2}\frac{\partial^2 p'}{\partial t \partial y} - \frac{1}{\rho_0^2 f_0^3} J(p', \frac{\partial p'}{\partial y}) - \frac{\beta_0}{\rho_0 f_0^2} y \frac{\partial p'}{\partial x}. \tag{25b}$$

The velocities from eq. 25 can be related to the stream function ψ thorugh $p' = \rho_0 f_0 \psi$,

$$u = -\frac{\partial \psi}{\partial y} - \frac{1}{f_0}\frac{\partial^2 \psi}{\partial t \partial x} - \frac{1}{f_0} J(\psi, \frac{\partial \psi}{\partial x}) + \frac{\beta_0}{f_0} y \frac{\partial \psi}{\partial y}, \tag{26a}$$

$$v = \frac{\partial \psi}{\partial x} - \frac{1}{f_0}\frac{\partial^2 \psi}{\partial t \partial y} - \frac{1}{f_0} J(\psi, \frac{\partial \psi}{\partial y}) + \frac{\beta_0}{f_0} y \frac{\partial \psi}{\partial x}, \tag{26b}$$

where the first term of both expressions corresponds to the geostrophic velocity and the rest to the ageostrophic velocity.

Once we have developed the velocity expressions, it is trivial to obtain the horizontal divergence and vorticty from the expressions in eq. 27 and eq. 28,

$$D = \frac{\partial u}{\partial x} + \frac{\partial v}{\partial y}, \tag{27}$$

$$\zeta = \frac{\partial v}{\partial x} - \frac{\partial u}{\partial y}. \tag{28}$$

Appendix C

Trajectory of the whole cluster of drifters

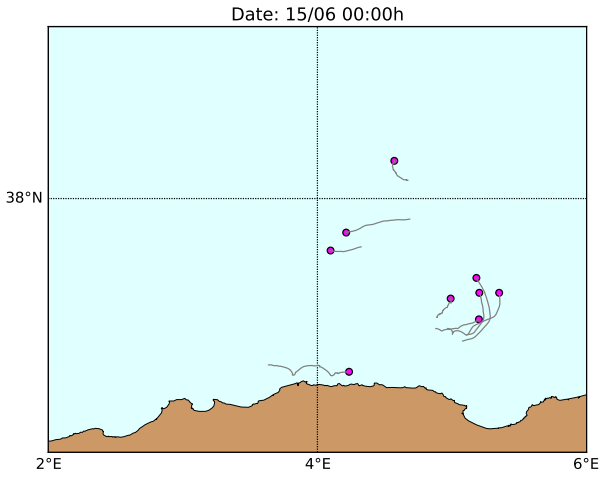

(a)

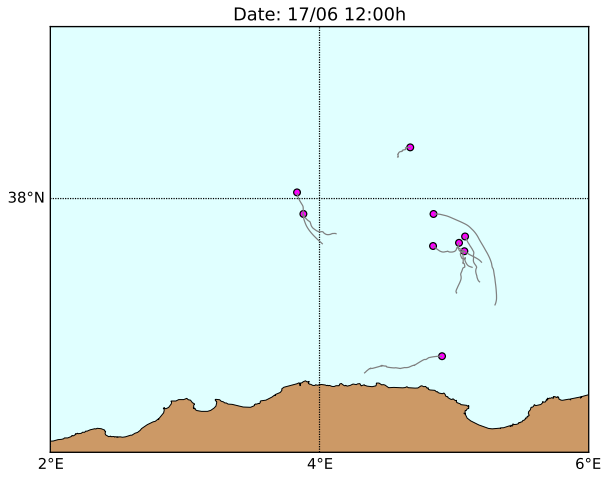

(b)

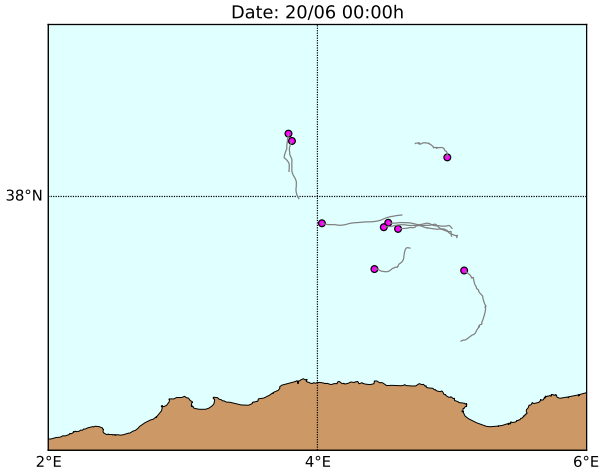

(c)

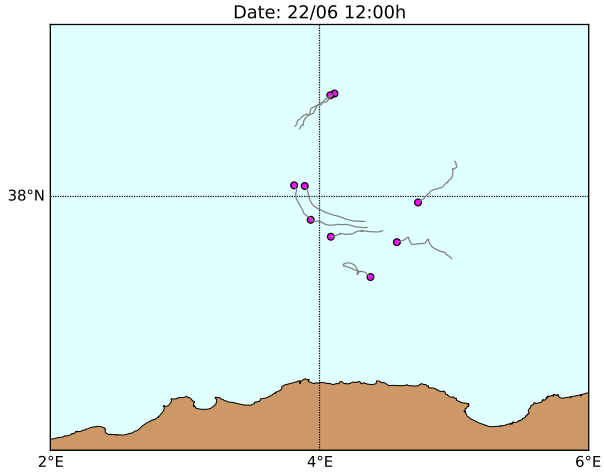

(d)

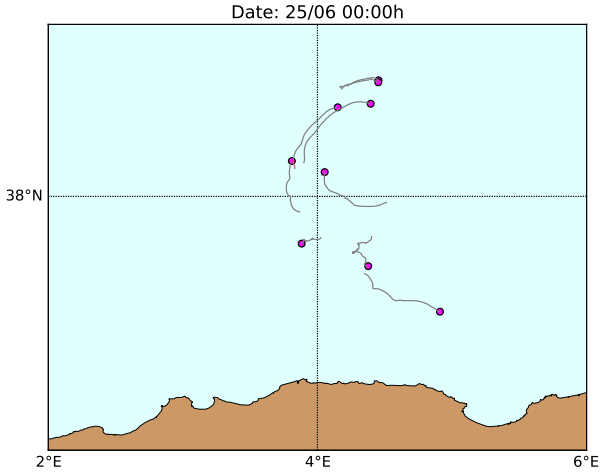

(e)

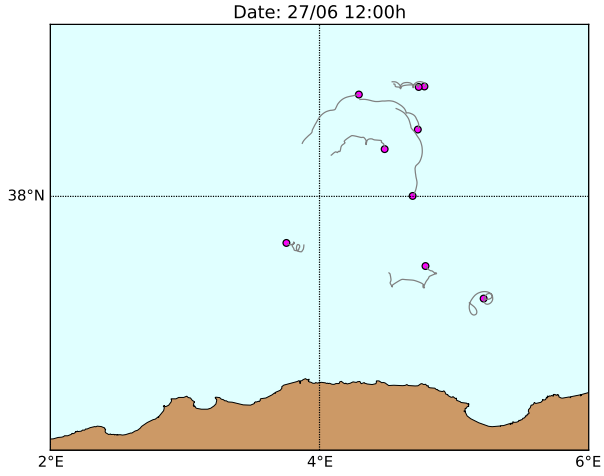

(f)

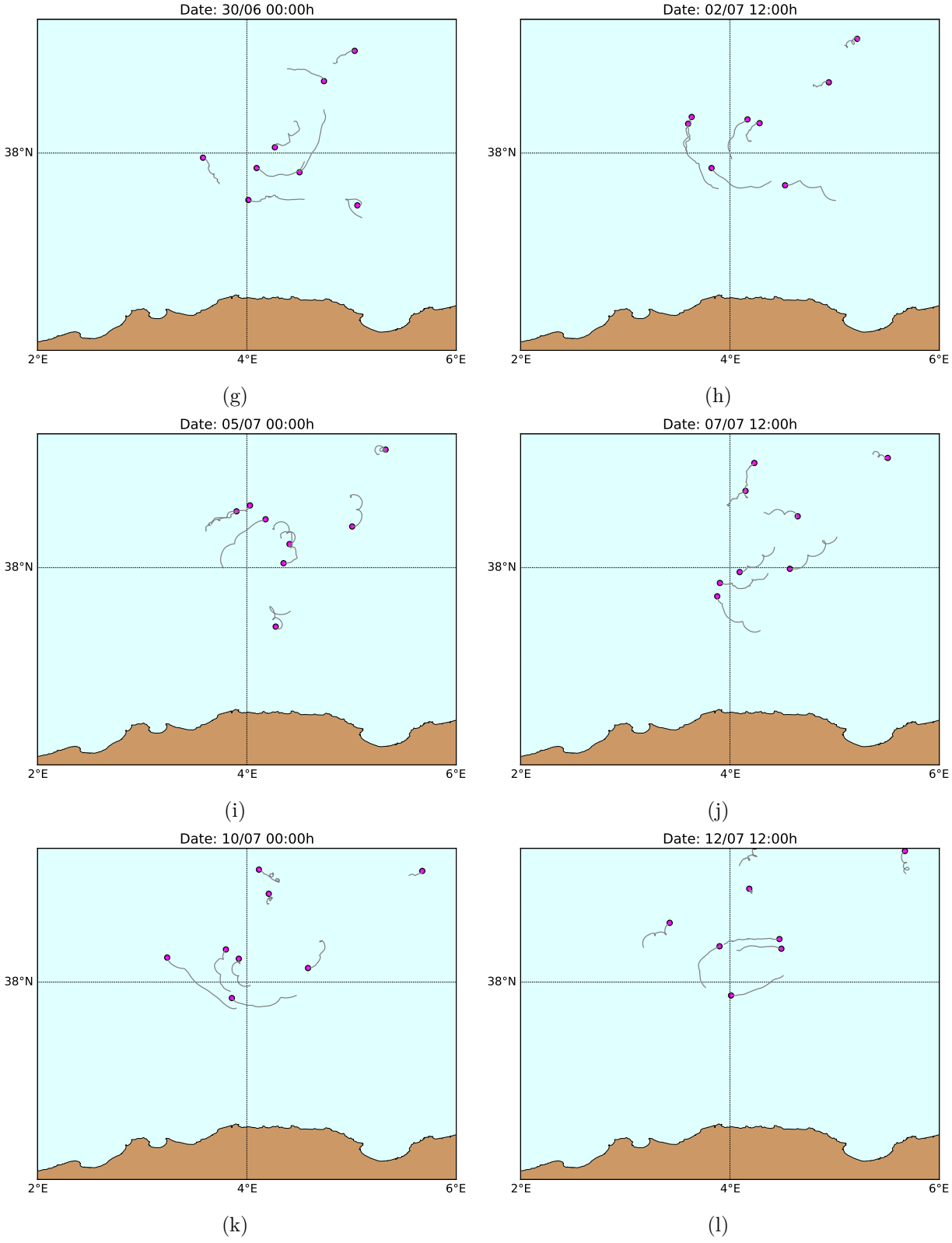

(g) (h) (i) (j) (k) (l)

Figure 18: Trajectory of all the drifters that sampled the eddy

Trajectory of the drifters inside the eddy

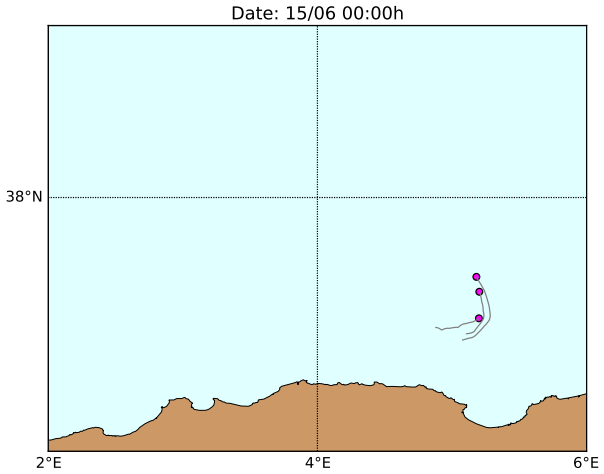

(a)

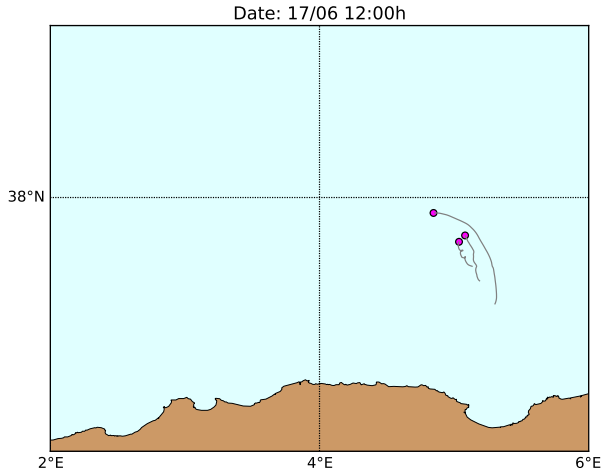

(b)

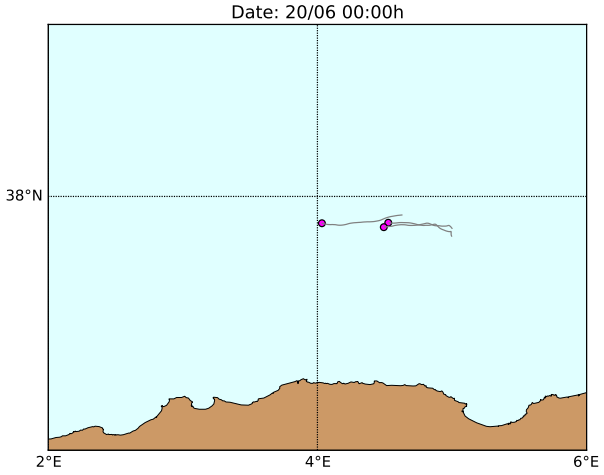

(c)

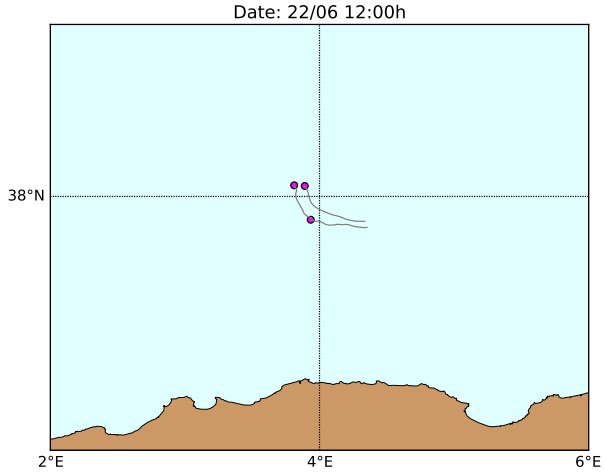

(d)

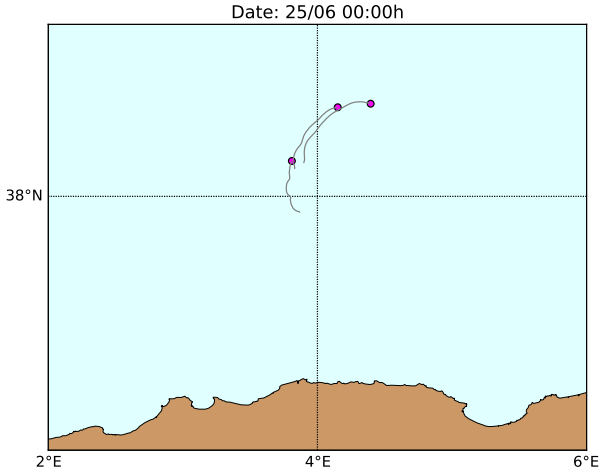

(e)

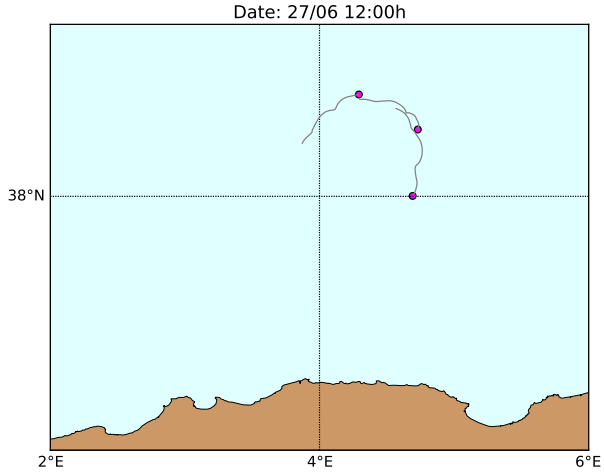

(f)

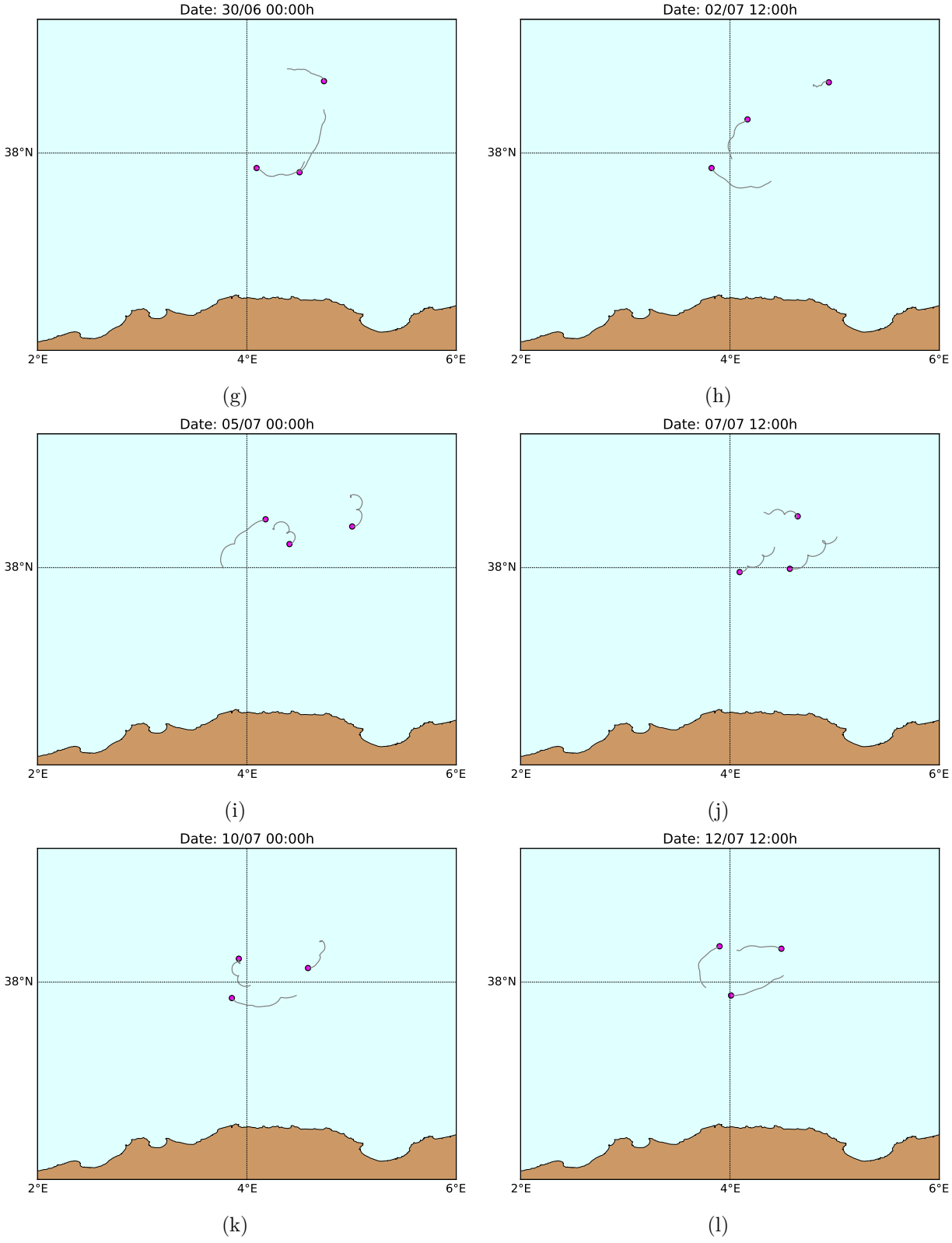

(g) (h) (i) (j) (k) (l)

Figure 19: Trajectory of the three drifters selected to apply the triangle method.

Appendix D

Dynamic height field evolution

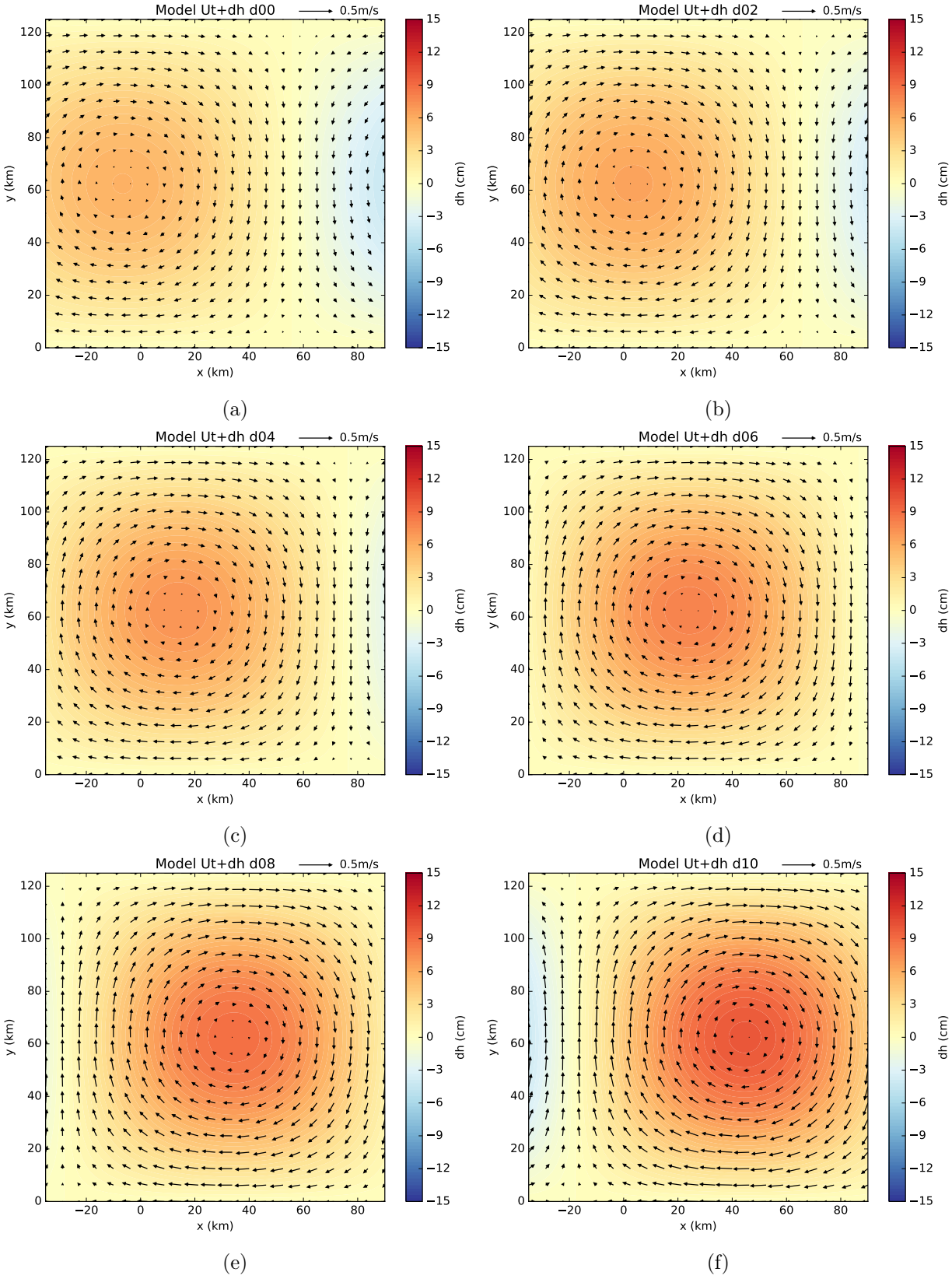

Figure 20: Time evolution (in days) of the dynamic height field (filled contour plot) with the velocity field (vector plot) on top.

Geostrophic and ageostrophic velocity field evolution

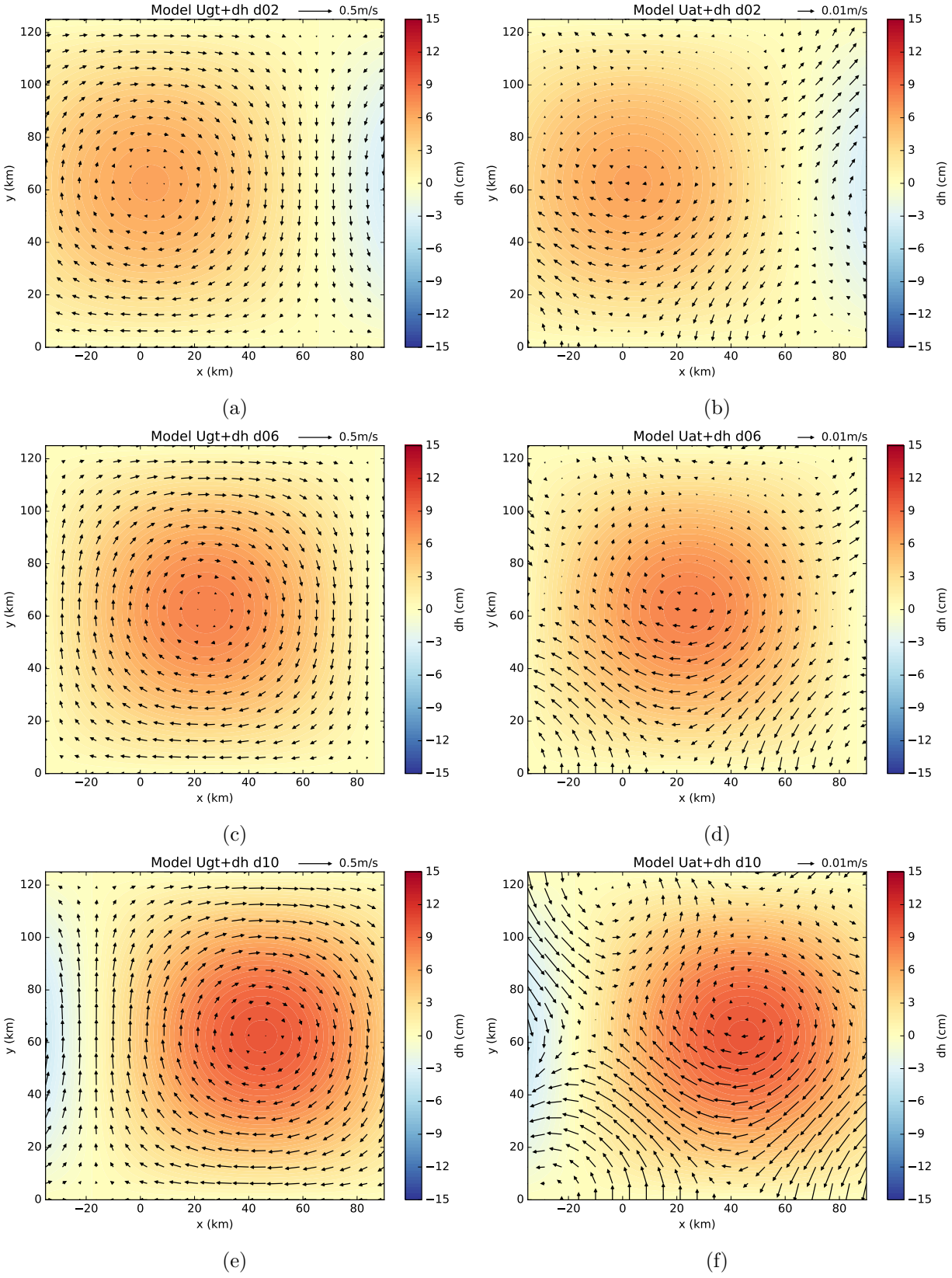

Figure 21: Time evolution (in days) of the dynamic height field (filled contour plot) with the geostrophic ((a)-(c)-(e)) and ageostrophic ((b)-(d)-(f)) velocity fields (vector plot) on top.

Divergence and vertical velocity field evolution

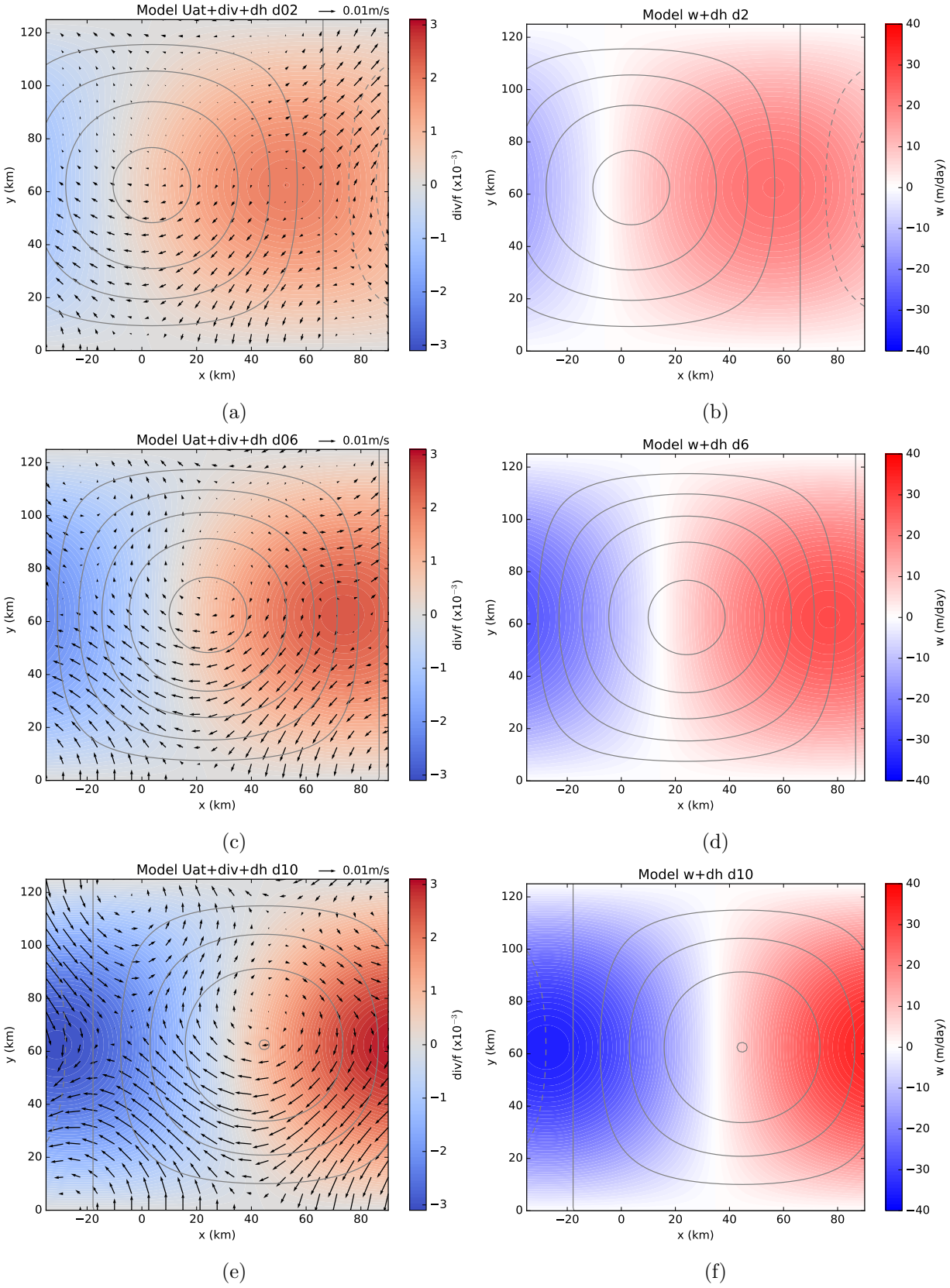

Figure 22: Time evolution (in days) of the divergence field (filled contour) with the ageostrophic velcity on top (vector plot) and dynamic height (contours) ((a)-(c)-(e)) and vertical velocity field (filled contour) with dynamic height (contours) on top ((b)-(d)-(f)).

List of Figures